CHEMICAL REVIEWS

REVIEW

pubs.acs.org/CR

Role of Molecular Order and Solid-State Structure in Organic Field-Effect Transistors

Marta Mas-Torrent* and Concepció Rovira*

Institut de Ciència de Materials de Barcelona (ICMAB), Consejo Superior de Investigacions Científicas (CSIC), Campus UAB, 08193 Bellaterra, Spain

Networking Research Center on Bioengineering, Biomaterials and Nanomedicine (CIBER-BBN), ICMAB-CSIC, 08193 Bellaterra, Spain

CONTENTS

1. INTRODUCTION: ORGANIC FIELD-EFFECT TRANSISTORS

The invention of the transistor in 1947 by John Bardeen, William Shockley, and Walter Brattain is regarded as one of the greatest discoveries of the 20th century since it is the basic component in modern electronics. Since the first Ge-based device a few centimeters in size, the microelectronics industry has developed rapidly, and microprocessors with hundreds of millions of transistors are currently fabricated. However, due to the fact that inorganic electronics have some technological limitations associated with them, organic-based devices have recently emerged in the market, beginning to replace amorphous silicon in some applications, and also have great possibility to find their place in a wide range of new applications. One of their main advantages is solution- processability, and thus, organic materials offer the possibility to fabricate low-cost and flexible devices and are also suitable for large area applications. This has been the motivation for why this field has been labeled "organic and large area electronics (OLAE)". In addition, the versatility of organic synthesis allows for the preparation of materials "à la carte". That is, since by chemically modifying their molecular structure and functionality the solid-state structure and the resulting macroscopic properties are altered, it is feasible to synthesize tailored materials for specific uses.

The operation principle of an organic field-effect transistor (OFET) relies on the application of an electric field that causes the formation of a conducting channel in the dielectric/semiconductor interface. The two main configurations employed in OFETs are depicted in Figure 1 and are known as *top contact* and *bottom contact*. In both cases, the organic semiconductor deposited on a dielectric is contacted with two metal contacts, namely, the *source* and *drain*, and on the other side of the dielectric a third contact, the *gate*, is placed. Thus, the source−drain current (I_{SD}) flowing along the organic material can be modulated by application of a gate voltage (V_G) between the source and the gate, which creates an electric field responsible for the formation of an accumulation layer of charges at the semiconductor/dielectric interface. Also, depending on the V_G applied, the nature of the charge carriers accumulated at the interface can be controlled, that is, holes (in p-type semiconductors) or electrons (in n-type semiconductors).

In a simplified way, the operation of an OFET can be explained as follows. The voltage applied to the gate shifts the highest occupied molecular orbital (HOMO) and lowest unoccupied molecular orbital (LUMO) energy levels with respect to the metal Fermi level (E_F) of the source−drain contacts, which allows for the formation of the conducting channel (Figure 2). Hence, a negative gate voltage shifts the orbitals up and might result in the alignment of the HOMO with E_F, making it possible to have hole conduction. Otherwise, if a positive gate voltage is applied, the HOMO and LUMO will shift down, and if the LUMO becomes resonant with E_F, electrons will flow from

Received: May 14, 2010
Published: March 18, 2011

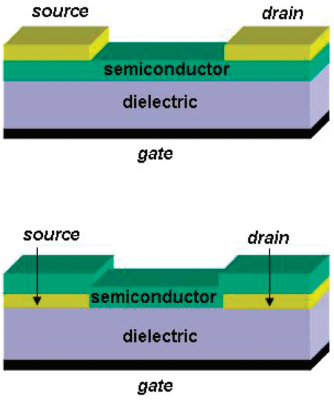

Figure 1. Common OFET configurations employed: top contact (top) and bottom contact (bottom).

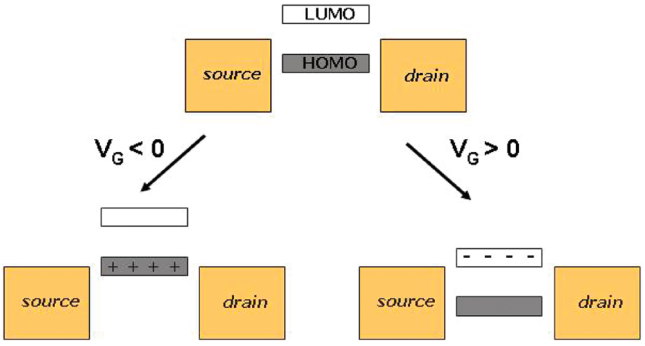

Figure 2. Schematic representation of the HOMO and LUMO of the organic semiconductor with respect to the source−drain metal Fermi level.

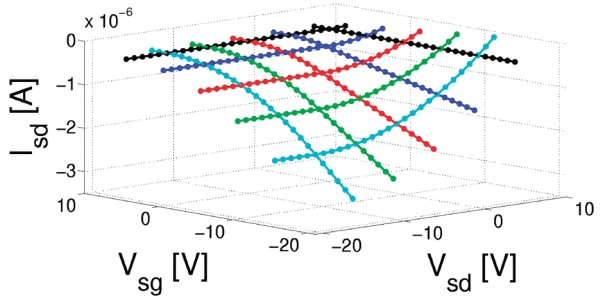

Figure 3. Theoretical transport properties from a p-type OFET.

the metal to the LUMO. However, one should bear in mind that the orbital shifting induces bending of the bands near the source−drain electrodes and, thus, there is an energy barrier at these contacts.

The calculated electrical characteristics obtained in an OFET are shown in Figure 3. In general, the OFET transport properties are described with two types of graphs. The output characteristics correspond to the representation of the I_{SD} versus the V_{SD} at fixed V_G. In this plot, it is clearly observable that there are two regimes, the linear regime, where the current is described by a parabola, and the saturation regime, where the source−drain current is independent of the source−drain voltage. Additional information can be extracted from the transfer characteristics, which plots the I_{SD} with the V_G at fixed V_{SD}. Here, the on/off ratio, which is the ratio of current in the accumulation mode to the current in the depletion mode, and the threshold voltage (V_T), that is, the gate voltage from which the conduction channel starts to form, can be easily visualized. A few reviews have already been published stressing the physics and operation mechanisms of OFETs.[1]

The performance of an OFET is mainly determined by the charge carrier mobility (μ), which has been improved enormously since the fabrication of the first OFET over 20 years ago. This parameter can differ by orders of magnitude depending on the materials used for the semiconducting channel. Poorly conducting organic semiconductors have mobilities of 10^{-4} $cm^2/(V\ s)$ or lower, good-quality organic materials have mobilities of $\sim 10^{-2}$ $cm^2/(V\ s)$, and well-ordered organic materials have mobilities in the range of $\sim 1-10$ $cm^2/(V\ s)$. Amorphous silicon has a mobility of ~ 1 $cm^2/(V\ s)$, crystalline silicon has mobilities on the order of $\sim 10^3$ $cm^2/(V\ s)$, and exceptionally clean systems of inorganic semiconductors can have mobilities of 10^7 $cm^2/(V\ s)$. Thus, considering the OFET mobilities commonly achieved currently,[2] it is evident that organic devices will not be suitable to fabricate high-speed components but they can compete with amorphous silicon applications.

There are a large number of factors that affect the device performance, and therefore, the comparison of measurements performed in different laboratories should be carried out with caution. For instance, the choice of metal electrodes affects the contact resistance, since it is important to choose the electrode metal according to the nature of the organic semiconductor to have efficient charge injection.[3] The dielectric material influences the electric field created along it, the current leakage through the gate insulator, and also the charge trapping.[4] It is also well-known that both organic semiconductor/metal and organic semiconductor/dielectric interfaces have a strong impact on the molecular and mesoscale structures.[5] Molecular self-assembled monolayers (SAMs) on the metal electrodes and on the dielectric have been proved to be a useful tool to control the charge injection and the molecular order.[6] Likewise, the device configuration will also affect the OFET properties. Finally, the choice of the organic semiconductor will be key to achieve a high mobility.

There are two main families of organic semiconductors that can be used in OFETs: (i) conjugated polymers (e.g., polyphenylene, polythiophene, poly(phenylenevinylene)) and (ii) small conjugated molecules with low molecular weight (e.g., pentacene, oligothiophene, tetrathiafulvalene). In both cases, the conductivity is determined by the relative position of the $\pi-\pi$ orbitals. Since in organic semiconductors the intermolecular van der Waals interactions are much weaker than the covalent interatomic bonds found in inorganic semiconductors such as silicon, thermal fluctuations disrupt the molecular order and result in lower mobilities than the ones observed in their crystalline inorganic counterparts. For this reason, while the charge transport in inorganic semiconductors takes place via delocalized states following a band transport regime in which the conductivity is limited by the lattice vibrations, it is generally agreed that, at least at room temperature, the charge mobility of organic semiconducting materials is determined by a hopping transport process, which can be depicted as an electron or hole transfer reaction in which an electron or hole is transferred from one molecule to the neighboring one. According to Marcus theory, two major parameters determine self-exchange rates and,

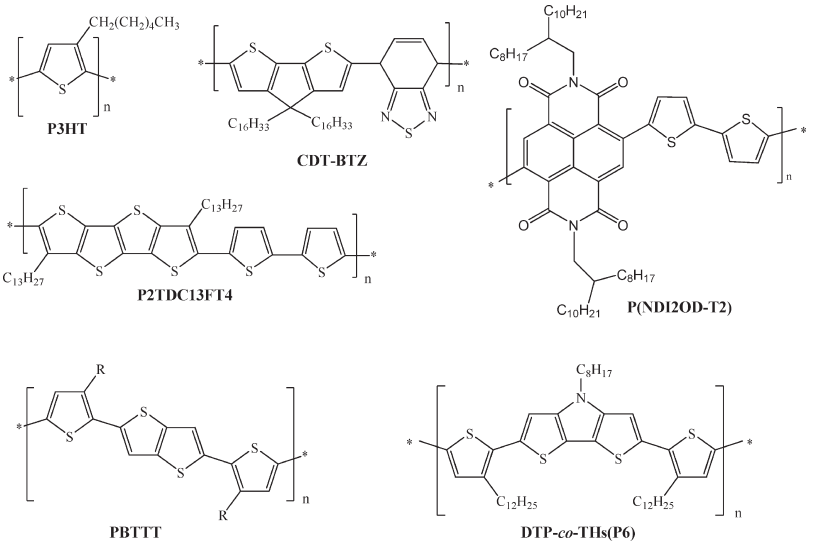

Figure 4. Conjugated polymers employed for the fabrication of thin-film OFETs.

thus, the charge mobility:[7] (i) the electronic coupling between adjacent molecules (t), which needs to be maximized, and (ii) the reorganization energy (λ_{reorg}), which needs to be small for efficient charge transport.[8] The electronic coupling t reflects the strength of the interactions between the electronic levels (HOMO for holes and LUMO for electrons) of the molecules involved in the charge transfer process.[9] λ_{reorg} depicts the changes in the geometry of the two molecules during the electron transfer reaction.[8] It has two contributions, an internal one (λ_i) that is often computed at the density functional theory (DFT) level, giving values in good agreement with the ones extracted from ultraviolet photoemission spectra,[10] and an external one (λ_s) that accounts for the nuclear displacements in the surrounding medium and the resulting electronic effects.[11] This parameter cannot be easily accessed from quantum-chemical calculations, though estimations are obtained from simple models based on a dielectric continuum.[12] In addition, a theoretical study showed that when the local molecular environment is taken into account (i.e., including in the calculation a cluster of molecules instead of a single one) and the charge can be partially delocalized over several molecules, the value of the reorganization energy is significantly affected.[13,14] All this elucidates the primary importance of intermolecular interactions on the hopping mobility.

Considering all of the above discussion, it is obvious that the choice of the organic semiconductor will mainly determine the device performance and, therefore, it will be important to take into account the intermolecular interactions that the molecules exhibit, as the stronger the electronic coupling between neighboring molecules, the higher the mobilities achieved. However, the correlation of the molecular order and crystal structure with the device performance to fully understand the transport mechanisms and to facilitate the design of new promising semiconductors still remains an extremely complex subject. Careful theoretical and experimental studies have been carried out pursuing this purpose, but often theory and experiments do not match, elucidating that there is a lot of work needed to understand the transport mechanisms and develop advanced performance devices.

The main goal of this review is to highlight the influence of the molecular organization on the mobility of OFETs, with emphasis on some of the factors that should be bore in mind, such as polymorphism, intermolecular interactions, and interfaces.

2. MORPHOLOGY AND MOLECULAR ORDER IN THIN-FILM TRANSISTORS

In thin-film OFETs, in addition to the local intermolecular interactions, the film morphology will strongly influence the charge transport. Great efforts are therefore being devoted to control the local intermolecular ordering as well as the mesoscopic film morphology[15] in both polymer thin films (Figure 4) and films based on small conjugated molecules (Figure 5).

2.1. Polymers

Devices fabricated with thin-film polymers have more potential applications due to their solution processability. However, polymers form typically complex microstructures, where microcrystalline domains are embedded in an amorphous matrix, which limits charge transport.[16] The most studied polymer for OFETs has been regioregular poly(3-hexylthiophene) (P3HT; Figure 4), which has given one of the highest OFET mobilities ($0.1-0.2\ cm^2/(V\ s)$) found for an organic polymer OFET.[17−19] This high mobility is ascribed to structural order in the polymer film induced by the regioregular head-to-tail coupling of the hexyl side chains, which results in a lamellar structure (Figure 6).[20] The microstructure of P3HT, in addition to the degree of regioregularity, depends on the deposition conditions and the molecular weight (i.e., the average polymer chain length). The dynamic self-organization of this polymer during the process of going from the solution to the solid-state phase is greatly influenced by the deposition method employed. Thus, the drop-casting technique tends to give rise to higher OFET mobility than spin-coating.[21] On the other hand, the best mobility has been achieved by employing the dip-coating deposition method.[19] Additionally, depending on the solvent employed, P3HT can form fibers in solution, which can then be deposited on the substrate.[22] Hole mobilities in the range of $0.02-0.06\ cm^2/(V\ s)$ have been reported for single nanofibers and films of fibers aligned by applying an ac voltage.[23] The formation of similar fibers has also been observed in other

dx.doi.org/10.1021/cr100142w |Chem. Rev. 2011, 111, 4833–4856

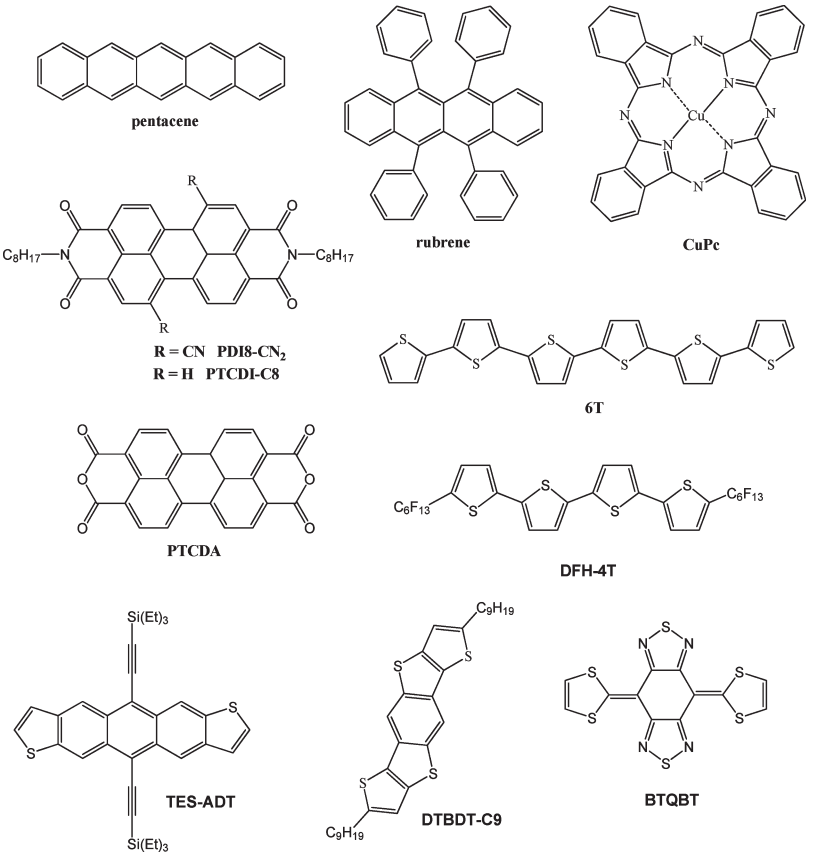

Figure 5. Small conjugated molecules employed for the fabrication of thin-film OFETs.

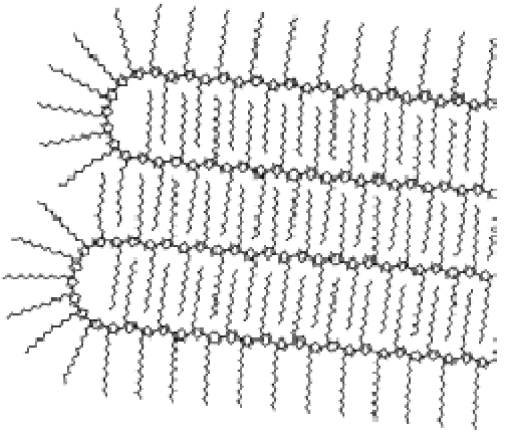

Figure 6. Schematic lamellar-type ordering in P3HT films. Reprinted with permission from ref 20. Copyright 2000 Wiley-VCH Verlag GmbH & Co.

conjugated polymers and is believed to be governed by the π stacking of the conjugated chains.[24] It has also been reported that the molecular weight has an impact on the film morphology. It is known that, in small molecular weight P3HT, crystalline fibers are formed by the face-to-face interactions of the polymer chains. By increasing the molecular weight, the fiber morphology evolves into a nodular structure with chain folding and lower crystallinity. However, the OFET mobility in P3HT is found to increase with the molecular weight, which is attributed to the improved interconnectivity between the domains. That is, although the lower molecular weight polymers form larger crystalline domains, the pronounced grain boundary sites act as deep charge trapping sites for transport hindering, thus the resultant OFET mobility of the films.[25]

Mechanical techniques have also been used to promote film ordering in P3HT. The *friction transfer* technique has been shown to be promising for preparing molecularly arranged films without involving solution processes.[26] Efficient molecular orientation at the nanometer scale in P3HT films has also been achieved by the *nanorubbing* technique with an atomic force microscopy (AFM) stylus.[27] Moreover, the use of a directional crystallization technique that takes advantage of 1,3,5-trichlorobenzene acting first as a solvent and second as a substrate for polymer epitaxy permits the preparation of regioregular P3HT films that are highly anisotropic in-plane.[28]

In addition to P3HT, a variety of thiophene-based polymers have also been reported for the fabrication of OFETs, and different approaches to engineer higher performance have also been focused on improving the packing. One example is the copolymer poly(2,5-bis(thiophene-2-yl)-3,7-ditridecanyltetrathienoacene, P2TDC13FT4) designed to increase the rigidity of the thiophene monomer through the use of an alkyl-substituted core that consists of four fused thiophene rings (Figure 4).[29] This polymer exhibited a field-effect hole mobility exceeding 0.3 $cm^2/(V\,s)$. Polymers with elevated molecular weight have also been proved to have higher macroscopic order, reducing the number of trapping or scattering sites, such as cyclopentadithiophenebenzothiadiazole copolymer (CDT-BTZ;

Figure 4), which reached a mobility of up to 0.67 $cm^2/(V\ s)$ in films prepared by spin-coating followed by an annealing step.[30] This is in contrast to what is observed with P3HT films that show higher crystalline domains with shorter polymer chains. A different strategy followed recently to obtain polymers with increased structural order has been the use of polymer liquid crystals.[18] OFETs based on the liquid crystal poly(2,5-bis-(3-alkylthiophene-2-yl)thieno[3,2-*b*]thiophene (PBTTT; Figure 4) have led to mobilities as high as 0.7 $cm^2/(V\ s)$ in the mesophase.[31]

Despite this interest in preparing polymers that show long-range-ordered structures, some examples of amorphous films have been described to exhibit remarkably high OFET mobilities. For instance, mobilities of 10^{-2} and 0.17 $cm^2/(V\ s)$ were found for a poly(triarylamine) thin film[32] and for a low molecular weight CDT-BTZ copolymer,[33] respectively, and more recently, for films of a conjugated copolymer based on *N*-alkyldithieno-[3,2-*b*:2′,3′-*d*]pyrroles and thiophene units (DTP-*co*-THs(P6); Figure 4), a mobility of up to 0.21 $cm^2/(V\ s)$ has been reported.[34]

All the previously mentioned polymers belong to p-type semiconductors, since the progress in OFETs using n-type semiconductors is still far from the performance achieved with p-type materials. However, very importantly, a new n-type polymer based on a naphthalenebis(dicarboximide) (Figure 4, P(NDI2OD-T2) has been reported to show a very high electron mobility (0.45−0.85 $cm^2/(V\ s)$) together with solution processability and air stability.[35] Surprisingly, the wide-angle X-ray diffraction (XRD) scans of these films reveal negligible Bragg reflection intensities, indicating also the amorphous nature of these films.

In principle, disordered films are not expected to be suitable for charge transport due to the presence of numerous charge carrier trapping sites, although some theoretical models have tried to explain charge transport in such disordered media.[1a,36] The high OFET performance obtained for the poly(triarylamine) amorphous films was explained by the lower degree of energetic disorder, which was achieved by employing a nonpolar dielectric that provided uniform charge transport paths. In any case, the exceptionally facile processability of amorphous films makes them extremely appealing for introducing organic devices into the market.

2.2. Small Conjugated Molecules

The importance of the molecular ordering for fabricating OFETs with high performance is even more important in small-molecule-based transistors. Small molecules, which are more commonly deposited employing vacuum deposition techniques due to their lower solubility in organic solvents, can also form films with a variety of crystallinity degrees and even exhibit different solid-state structures. For instance, Dimitrakopoulos and Mascaro demonstrated that films of pentacene evaporated at different temperatures show a range of crystallinities that correlate with the resulting OFET performance.[37] The influence of the substrate temperature was also investigated in thin films of copper phthalocyanine (CuPc; Figure 5), and a strong impact on the film morphology was observed, which went from grains to rodlike and large flat crystals with increasing temperature (Figure 7).[38] Although large crystals are expected to be more optimum for the electronic transport, at high temperature the nucleation was sparse and the large crystals were not well-interconnected. Thus, the best device performance was achieved here for an intermediate temperature (120 °C), indicating the

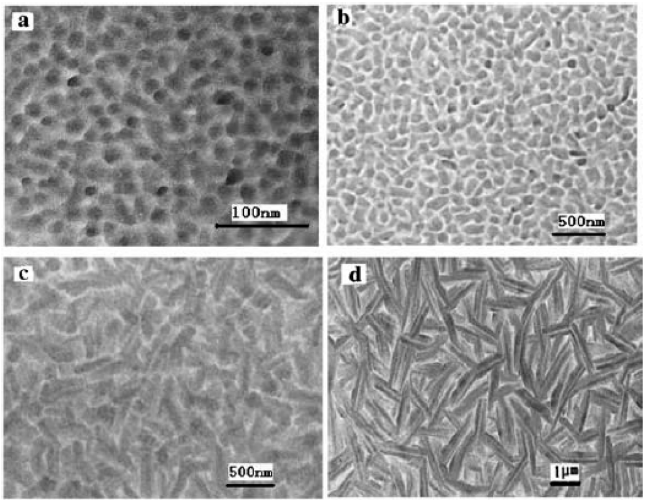

Figure 7. Transmission electron images from CuPc films deposited at (a) T_{sub} = 20 °C, (b) T_{sub} = 120 °C, (c) T_{sub} = 170 °C, and (d) T_{sub} = 200 °C. Reprinted with permission from ref 38. Copyright 2003 Springer.

importance not only of the grain size but also of the film homogeneity. On the other hand, we should also mention that recently Salleo and co-workers reported that the device performance can be optimized by controlling the grain boundary orientation or reducing the energetic barrier associated with transport across less favorable boundaries.[39] They found that in films based on the perylenediimide semiconductor PDI8-CN_2 (Figure 5) the grain boundary orientation modulates by about 2 orders of magnitude the charge mobility and also that the molecular packing motif is crucial in the grain-boundary-induced anisotropy.

There are other parameters during the evaporation of the organic semiconductor that also affect the molecular solid-state structure and, hence, the device performance. For example, the deposition rate affects the nucleation density.[40] Generally, a slower deposition rate results in a lower nucleation density and large grains, which are favorable for charge transport. However, there are exceptions to this rule since variations of these parameters can also lead to modification of the crystal structure (see the section "Polymorphism"). Accordingly, the investigation of the molecular beam deposition of pentacene and bis(1,2,5-thiadiazolo)-*p*-quinobis(1,3-dithiole) (BTQBT; Figure 5) revealed that these materials show higher OFET mobility when they are deposited at a high rate due to the presence of mixed phases at a low deposition rate in the case of pentacene[41] and the improved molecular ordering in BTQBT at higher deposition rates.[42]

Another clear example of the influence of all the previously mentioned deposition parameters on the film morphology and, as a consequence, on the device mobility has very recently been described by Facchetti and Marks.[43] They synthesized a series of benzo[*d*,*d*]thieno[3,2-*b*;4,5-*b*]dithiophene (BTDT) derivatives and prepared OFETs with thin films of these molecules on bare SiO_2 and on octadecyltrichlorosilane (OTS)-treated SiO_2, varying the substrate temperature and deposition flux rate during the material evaporation. Since the trend in mobilities achieved within this series of semiconductors could not be accounted for by the calculated values of HOMO energies and the reorganization energies, as Marcus theory predicts, the authors

dx.doi.org/10.1021/cr100142w |*Chem. Rev.* 2011, 111, 4833–4856

investigated the film morphological and microstructural characteristics. They found for these BTDT molecules that the grain size increases with the substrate temperature and that higher deposition rates produce smaller but better interconnected crystalline domains. Finally, although hydrophobic substrates tend to result in larger grains, this was not obvious here, but instead, films on bare SiO_2 exhibited larger voids between the grains. By properly adjusting the deposition rate and substrate temperature of films deposited on OTS-SiO_2, an efficacious compromise between high film crystallinity and efficient grain interconnectivity was achieved, making it possible to significantly modify the device performance and reaching a maximum OFET mobility greater than 0.7 $cm^2/(V\ s)$.

Solution-based deposition methods have also been developed to prepare ordered films of small conjugated molecules, and similarly, investigations concerning the influence of the deposition parameters on the film morphology have also been carried out.[44] In the past few years, techniques such as zone-casting,[45] dip-coating,[46] solution-sheared deposition,[47] or a combination of capillarity−wetting techniques[48] have successfully been employed to grow from solution crystalline oriented films or stripes of the organic semiconductors.

An elegant approach based on supramolecular chemistry has recently been published by Fréchet and Xu.[49] They show that the noncovalent linking of an organic semiconductor to a polymer chain allows solution processing and ordering of semiconductor molecules into hierarchical assemblies with macroscopic alignment of the organic semiconductor in thin films.

2.3. Postdeposition Treatments

Furthermore, the thin-film morphology can also be improved after deposition regardless of the method employed to deposit the organic material (i.e., solution or vacuum) or the material nature (i.e., polymer or small molecule). Temperature annealing is commonly used since it gives energy to the molecules to reorganize. Polymers can be annealed at around or above the glass transition and oligomers below their melting point. Even at room temperature it has been observed that molecules can rearrange, as found in thin films of the semiconductor ((triethylsilyl)ethynyl)anthradithiophene (TES-ADT) that after seven days showed a 100-fold increase of the OFET mobility.[50] Interestingly, it has also been demonstrated that by using a vapor-annealing treatment the device performance can be improved since the solvent also facilitates the self-organization of the molecules.[51] More recently, a solvent-assisted reannealing process based on the introduction of a small amount of solvent into a polymer film followed by a heating process has also been proved to significantly help the device performance.[52]

An alternative attempt to utilize high-quality organic semiconductor crystalline films to realize promising applicable devices has been reported.[53] This method consists in preparing a homogeneous mixture of an organic semiconductor (in this case, rubrene), a vitrifying diluent (1,2-diphenylanthracene) that hampers crystallization on casting from solution, and a high molecular weight polymer (atactic polystyrene) that provides good film-forming characteristics. When a hypereutectic mixture of the semiconductor and the glass-inducing species is annealed at a temperature above $T_{eutectic}$, crystallization of the semiconductor takes place. A very high OFET performance with a mobility of 0.7 $cm^2/(V\ s)$ has been obtained with this method, which could be extended for other organic semiconductors.

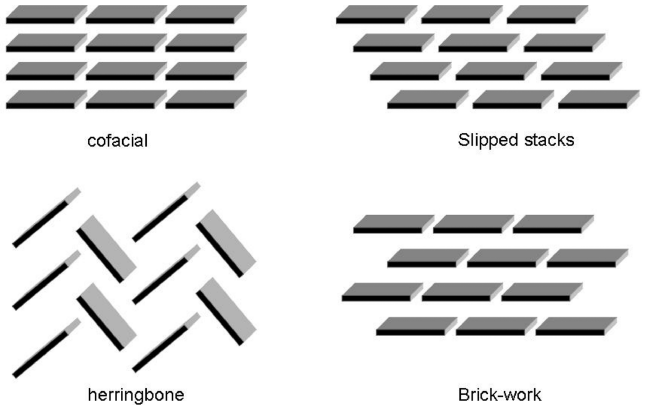

Figure 8. Some possible crystal packing motifs of conjugated organic molecules.

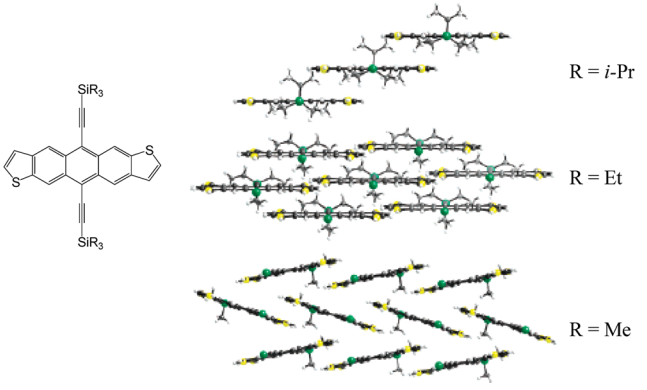

Figure 9. Crystalline order of anthradithiophene derivatives. Reprinted from ref 55. Copyright 2005 American Chemical Society.

3. SOLID-STATE ORGANIZATION

The study of the influence of the crystal packing on the device performance is essential to design new promising materials. The structure−property correlation is still not well understood, although currently great efforts are being devoted in this direction, both theoretically and with experiments. The solid-state packing of the organic semiconductors depends on the nature of their conjugated electronically delocalized core together with the substituents that they might bear. However, it is extremely difficult to predict the solid-state order of the crystal-engineered molecules since small chemical modifications can cause a huge difference in the solid-state organization. Ideally, the investigation of the influence of the solid-state packing on the transport should be carried out in materials that are as similar as possible (i.e., molecular formula, type of intermolecular interactions, and electronic properties) and that only differ in crystal structure.

3.1. Crystal Packing Motifs: Herringbone versus Cofacial

Unsubstituted acenes and thiophenes tend to crystallize following a herringbone pattern, in which the molecules form 2D layers interacting face-to-edge through C−H···π interactions and minimizing the electrostatic π orbital repulsion (Figure 8). Although systems that can exhibit 2D conductivity are highly desirable for the fabrication of devices, intuitionally one would expect that if the molecules would adopt a more face-to-face arrangement, the electronic coupling would be

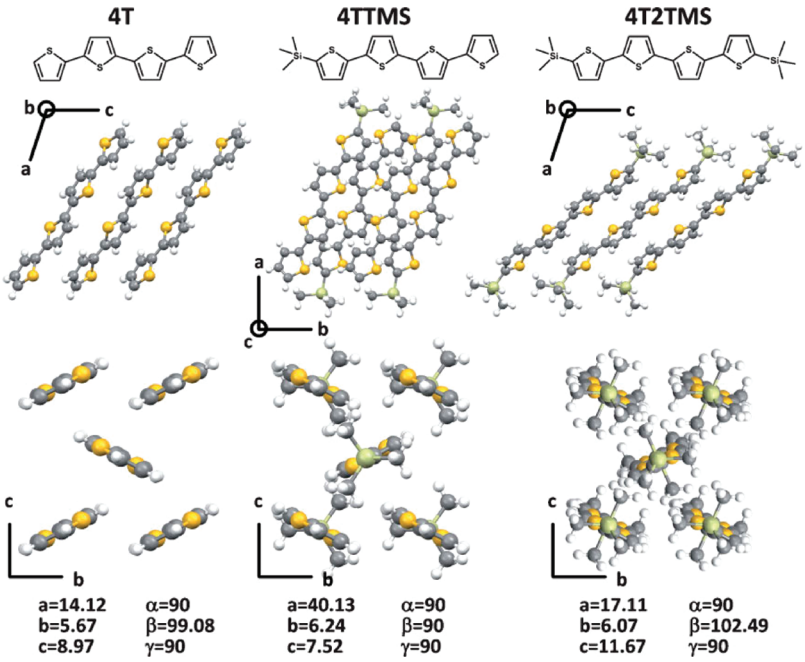

Figure 10. Chemical and crystal structures and lattice parameters of unsubstituted (4T), mono-TMS-substituted (4TTMS), and di-TMS-substituted quaterthiophene (4T2TMS). Terminal substitution determines the in-plane tilt (d) of the oligothiophene cores, with 4T2TMS (51°) > 4T (34°) > 4TTMS (26°). Reprinted with permission from ref 57c. Copyright 2009 Wiley-VCH Verlag GmbH & Co.

maximized due to enhanced $\pi-\pi$ overlap, and thus, the charge carrier mobility would also be improved. The addition of substituents to the conjugated core can indeed strongly modify the crystal packing of the organic semiconductors, forming slipped stacks, like in the high-mobility organic semiconductor rubrene, or brickwork arrays (Figure 8).[54] Interestingly, in the latter case, the 2D structure is preserved. Anthony and co-workers fabricated OFETs employing a series of anthradithiophenes that exhibit different packing depending on their chemical substitution (Figure 9).[55] It was observed that the (triethylsilyl)ethynyl-substituted anthradithiophene that crystallizes in a brickwork motif exhibited the highest charge carrier mobility (on the order of 1 $cm^2/(V\,s)$). On the other hand, the molecule that bears (triisopropylsilyl)ethynyl groups forms 1D slipped stacks when crystallized, whereas the one that is (trimethylsilyl)ethynyl-substituted forms the typical herringbone structure of unsubstituted acenes. The mobility found in the former case was lower than 10^{-4} $cm^2/(V\,s)$, and in the latter one no appreciable OFET characteristics were measured.

The bricklayer arrangement also proved to be very promising for the n-semiconductor 5,5′-bithiazole with (trifluoromethyl)-phenyl groups, which exhibited one of the highest reported electron mobilities of 1.83 $cm^2/(V\,s)$, while the mobility found in related materials with less favorable packing was much lower.[56]

Other works have also tried to rationalize the device performance obtained in oligothiophene and acene analogues in terms of the most favorable cofacial π stacking structure.[57] Depending on the substituents of tetracene or α-oligothiophene, different structures are obtained. Thus, monosubstituted 5- bromo- and 5-chlorotetracenes have the herringbone-type structure, while 5,11-dichlorotetracene[57a] and 5,6,11,12-tetrachlorotetracene[57b] have a face-to-face slipped π stacking motif. The mobilities of 5,11-dichlorotetracene and 5,6,11,12-tetrachlorotetracene were as high as 1.6 and 1.7 $cm^2/(V\,s)$, respectively, in single-crystal transistors, whereas 5-chlorotetracene displays a mobility 4 orders of magnitude lower.

A family of α-oligothiophene derivatives functionalized at the terminal positions with trimethylsilane (TMS) groups also display differences in the packing depending on the number of TMS substituents. In this case all adopt a layer-by-layer herringbone motif, but the tilt angle of the molecules within the *bc* plane varies with the terminal substitution (Figure 10).[57c]

The changes in the structure promote differences in the molecular overlap, which has a dramatic influence on the effective charge transport. Thus, the OFET performance decreases with substitution, being better for the device based on quaterthiophene (4T) and 1 order of magnitude lower for the one based on 4T2TMS. Interestingly, the predicted charge transport efficiency trend, 4T > 4TTMS > 4T2TMS, was coincident with the measured one.[58]

A nice study of the effect of very small changes in crystal structure on the performance of organic field-effect transistors has been developed by Minari et al. with a family of metalloporphyrin (2,3,7,8,12,13,17,18-octaethyl-21*H*,23*H*-metalloporphyrin, M-OEP) crystals with four different center metals, i.e., Co, Cu, Zn, and Pd. All compounds are isostructural, adopting the simple π stack structure along the *c* axis. The effect of the central metal is reflected in the intermolecular distance, which varies from 3.34 Å in Co-OEP to 3.41 Å in Pd-OEP. The field-effect mobility of the transistors measured along the stacking *c* axis is found to increase with decreasing intermolecular distance, which has been attributed to greater overlap of π orbitals among close-packed molecules and the consequent promotion of charge transport.[59]

Curtis and co-workers[60] also described the solid structure of a series of bithiazole and thiophene oligomers and substituted pentacenes employing the terminology "pitch and roll inclinations" from an ideal cofacial π stack. Pitch distortions are defined as shifts between adjacent molecules relative to one another in

dx.doi.org/10.1021/cr100142w |*Chem. Rev.* 2011, 111, 4833–4856

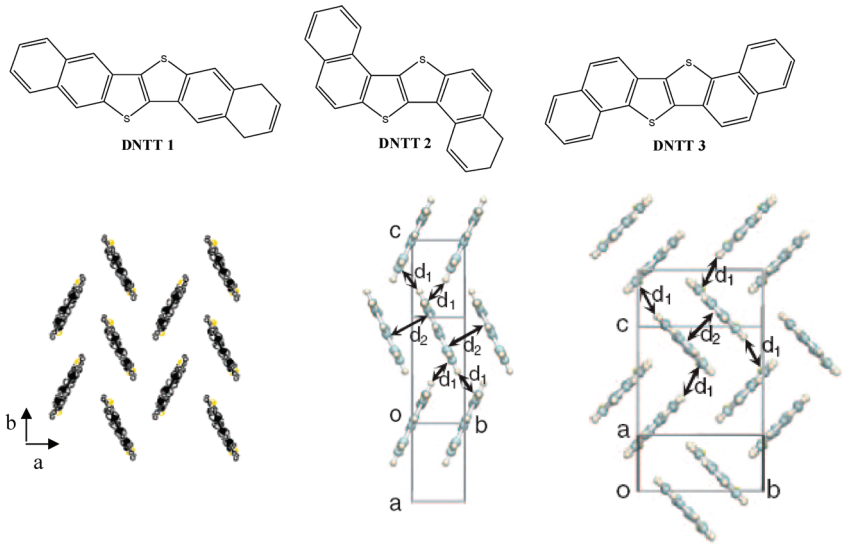

Figure 11. Molecular structure of the three DNTT isomers 1, 2, and 3 (top) and their crystal structures (bottom). Intermolecular distances: d_1(S···H) = 3.037 Å and d_2(π···π) = 3.536 Å for isomer 2; d_1(C···H) = 2.861 and 2.866 Å and d_2(π···π) = 3.434 Å for isomer 3. Reprinted from ref 62b. Copyright 2007 American Chemical Society.

the long molecular axis direction, whereas roll inclinations produce a translation along the short molecular axis. They state that moderately large pitch distortions do not disrupt $\pi-\pi$ interactions but roll displacements greater than 2.5 Å destroy the $\pi-\pi$ overlap between adjacent molecules. However, this chemical intuition regarding the favored cofacial stacking for transport in opposition to the herringbone packing has not been clearly demonstrated, and some theoretical studies predict that although cofacial oligomers show larger bandwidths, if the molecules are tilted, π overlap can be optimized and the electrostatic repulsion decreased.[61]

The formation of different crystal structures can be caused not only by the functionalization of the molecules but also by the isomer configuration chosen. A very illustrative example has very recently been reported by Takimiya and colleagues in which they reported three structural isomers of dinaphtho[2,3-*b*:2′,3′-*f*]thiopheno[3,2-b]thiophene (DNTT) (Figure 11).[62] Isomer DNTT 1 crystallizes following a herringbone pattern such as pentacene, while isomer DNTT 2 takes a simple π stack structure and DNTT 3 adopts the so-called sandwich herringbone structure in which dimers of molecules are packed in a herringbone manner. The formation of different crystal structures was attributed to the molecular shape that induced preferred intermolecular interactions. Thus, for linear isomer 1 the packing resembles that from acenes, while for the bent isomer 2 the herringbone packing motif is not favorable due to a reduced amount of face-to-edge C−H···π interactions. In the case of isomer 3, an intermediate situation is found. OFET thin-film devices exhibited a very high hole mobility of 3.0 $cm^2/(V\ s)$ for isomer 1, while for the other two isomers lower values of mobility were found ($10^{-2}-10^{-3}$ $cm^2/(V\ s)$), which was also primarily justified by the larger transfer integrals of DNTT 1. Again, the question of which crystal packing is more suitable for OFETs can be raised here; in this case the herringbone structure was the one leading to enhanced device performance instead of the cofacial one.

Further to the crystal packing motif, theoretical calculations also predict that the transfer integral values are extremely sensitive to the relative position of neighboring molecules.[61−63] As a consequence, small changes in the intermolecular distance and shifting or tilting of adjacent molecules can have a strong impact on charge transport.

3.2. Intermolecular Interactions

The molecular packing is certainly driven by the intermolecular interactions. In addition to the $\pi-\pi$ and C−H···π interactions which are commonly found in acene and thiophene analogues, there are other types of weak intermolecular interactions that can be used to tune the solid-state molecular arrangement and can play a crucial role. For instance, the semiconductor 2-(anthracen-9-ylmethylene)malonitrile was described to crystallize in a cofacial $\pi-\pi$ manner assisted by the hydrogen-bonding interactions between the cyanovinyl groups of neighboring columns.[64,65] When the cyano groups were replaced with methyl groups, no crystals were obtained, but when the methyl groups were replaced by carboxylic acids, the nanoribbon crystals grew again.

Halogen-based interactions, and in particular fluorine interactions, can also be exploited as supramolecular synthons. The partial fluorination of anthrathiophene semiconductors has been proved to help to accelerate crystallization thanks to the F···F and F···S interactions.[66] In addition, the approach of adding a few fluorine substituents did not affect the p-type transistor properties but improved the thermal stability and photostability of the materials.

Another type of molecular interaction widely employed in crystal engineering is the S···S interaction, which favors π stacking and can provide enhancement of the electronic dimensionality. The influence of such intermolecular interactions is clearly seen in hexathiapentacene, which when it crystallizes forms 1D stacks instead of following the herringbone motif typical of polyfused aromatic compounds.[67] An analogous situation was found when a sulfur atom was introduced into the perylene core.[68]

Furthermore, following an approach very much exploited in the field of organic conductors based on tetrathiafulvalene

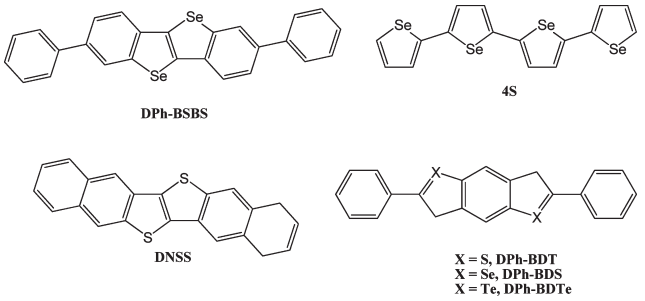

Figure 12. Organic semiconductors comprising Se or Te that have been employed for OFETs.

(TTF) charge transfer salts, Takimiya and collaborators have substituted the sulfur atoms in thiophene-comprising semiconductors with heavy chalcogen atoms such as selenium and tellurium (Figure 12).[69−71] These atoms are more polarizable and thus show enhanced overlap integrals. Of particular interest are the investigations of the OFET properties in the series of semiconductors DPh-BDX, where X is S, Se, and Te.[71] It was found that, as expected, the selenium homologue exhibited a mobility 1 order of magnitude higher than that of the sulfur one. However, the tellurium analogue had a lower performance, which was attributed to the lower aromatic nature of tellurophene rings causing less charge delocalization. We should, nevertheless, mention that this tendency of achieving a higher OFET mobility for Se-containing semiconductors compared to the sulfur derivatives has not been observed for the other studied materials.

3.3. Single-Crystal OFETs

Although the realization of low-cost organic electronic devices would entail the utilization of solution-processed materials that permit fabrication of films of large area coverage, the fundamental material characteristics of organic semiconductors are most clearly measured in single crystals. In addition, single-crystal OFETs[72] can be regarded as model systems to carry out correlation studies between crystal structure and device performance since in such devices parameters such as grain boundaries, alignment, film morphology, and crystallinity can be ruled out.

3.3.1. Fabrication. The fabrication of single-crystal OFETs is not straightforward due to the fact that the crystals are brittle and small. Also, most of the techniques used can easily damage the crystals, introduce contaminants, or produce traps at the interface and create barriers to the electron injection.[73,74] Two strategies have been followed to fabricate single-crystal OFETs. The first one is based on fabricating the transistor onto the organic crystal. This can be carried out by either painting the contacts with conducting graphite or silver paste or evaporating the metal electrodes through a shadow mask. In addition to the difficulty of fabricating contacts without breaking the crystals, this approach often implies the evaporation of the dielectric on the top of the crystal, which can create such a high density of defects on the organic surface that the field effect can be completely suppressed. The second strategy consists in placing the organic crystal or growing it directly on a prefabricated OFET structure. Its main advantage is that it is possible to employ the conventional lithography techniques applied in inorganic microelectronics, but on the other hand, it is also challenging to handle the fragile crystals or to grow them on a precise location.

Since most organic semiconductor oligomers are not very soluble, most of their single crystals have been prepared by

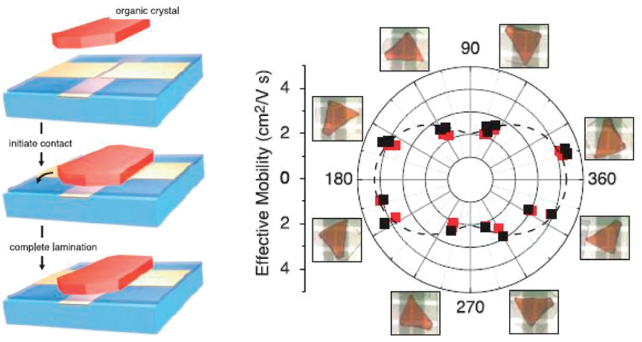

Figure 13. (a, left) Scheme of the lamination method of an organic single crystal on the surface of a substrate with source, drain, and gate electrodes. (b, right) Mobility at the rubrene $a-b$ surface (angle measured between the b axis and the conducting channel). The black and red squares correspond to the mobility calculated in the linear and saturation regime, respectively. Reprinted with permission from ref 78. Copyright 2004 AAAS.

sublimation of the organic material in a variety of vacuum deposition systems. The most common technique used to obtain organic single crystals is physical vapor transport,[73b,75] which is based on heating the source organic material placed on the hottest end of a glass or quartz tube submitted to a gradient of temperatures with an inert gas flowing along it. As the organic material is sublimed, it is carried down the tube by the gas and solidifies at its solidification temperature. Typically, the use of vapor phases allows for higher purity materials to be obtained, and hence, higher OFET mobilities have been achieved in this way. Morpurgo and colleagues reported OFETs of single crystals of tetracene obtained by physical vapor deposition that exhibited a hole field-effect mobility that reached 0.4 $cm^2/(V\ s)$ and of single crystals of a fluorocarbon-substituted dicyanoperylene-3,4:9,10-bis(dicarboximide) (PDIF-CN_2) with electron mobilities up to 6 $cm^2/(V\ s)$.[76,77] The fabrication process followed was the electrostatic adhesion of pregrown, free-standing crystals to a thermally oxidized Si wafer or a poly(methyl methacrylate (PMMA) dielectric on which source and drain electrodes had been deposited in advance. Additionally, OFETs based on single crystals of rubrene grown from the vapor phase have given mobilities of 15 $cm^2/(V\ s)$ using a polydimethylsiloxane (PDMS) dielectric[78] and up to 20 $cm^2/(V\ s)$ using air as the insulator.[79] These experiments were also performed by laminating the organic crystal on the surface of a substrate—in these cases, a polymeric PDMS stamp—on which the source, drain, and gate electrodes had been previously patterned (Figure 13a). In contrast with Si-based substrates that require very thin (on the order of 1 μm) and bendable crystals, the elastomeric stamps are compatible with much thicker (up to a few millimeters) and rigid crystals, as the flexible elastomeric surface adjusts easily to the crystal shape.[78]

Single crystals of organic semiconductors have also been prepared from solution by drop-casting a solution of the organic material on a substrate or dip-coating the substrate into the solution and allowing the solvent to evaporate. Here, parameters such as concentration, solvent, temperature, and evaporation rate play a crucial role in the size and quality of the crystals formed. For this strategy, TTF derivatives are attractive organic semiconductors[80] due to the fact that they are generally soluble in various solvents, contrary to the benchmark semiconductors pentacene and sexithiophene, which have to be chemically

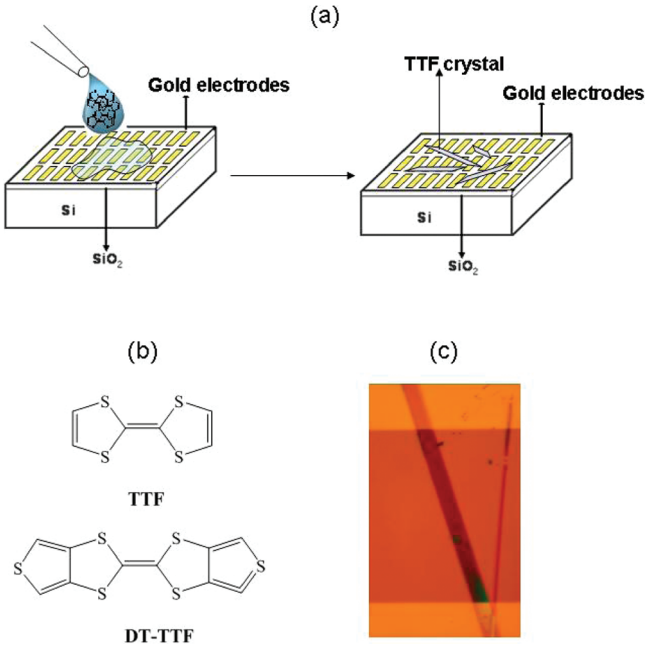

Figure 14. (a) Schematic procedure of integrating single crystals on prefabricated electrodes by drop-casting. (b) Molecular structure of TTF and DT-TTF. (c) Optical microscope image of a DT-TTF single crystal prepared by drop-casting lying on the gold electrodes. The width of the crystal is 30 μm.

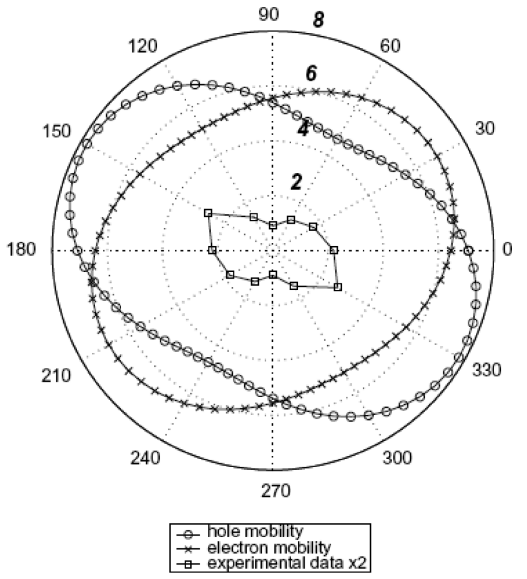

Figure 15. Polar plot of the calculated hole mobility, electron mobility, and experimental hole mobility at $V_G = -10$ V (from ref 85). The experimental values are multiplied by 2 for explicit contrast. The modeling electric field is 500 V/cm, and the density of charge carriers is 0.1/molecule. The italic bold numbers 2, 4, and 6 scale the mobility by the dashed circles, and the unit is cm^2/(V s). Reprinted with permission from ref 86. Copyright 2008 Elsevier.

modified to achieve solubility. Very high performance OFETs based on TTF crystals were prepared by drop-casting a solution of the TTF derivative onto the SiO_2 gate insulator and the prefabricated source and drain gold electrodes (Figure 14a).[81] The solution was allowed to evaporate slowly at room temperature in a chamber saturated with solvent vapors, which resulted in the formation of crystals randomly distributed on the substrate, some of which connected two of the microfabricated electrodes. Following this procedure, OFET mobilities of up to 3.6 cm^2/(V s) were reported for dithiophenetetrathiafulvalene (DT-TTF; Figure 14b,c).

Another possibility to fabricate solution-processed crystals for fabricating OFETs is the deposition of crystals formed already in a solution onto the device structure. For instance, high mobilities of 1.42 cm^2/(V s) were reported in devices using single-crystalline microribbons of bis((triisopropylsilyl)ethynyl)pentacene (TIPS-PEN).[82] The microribbons were prepared by the specific-solvent exchange method, which consisted in the injection of a concentrated solution of TIPS-PEN in toluene into acetonitrile, a solvent in which the molecule is not soluble. Also, OFETs with a maximum mobility of 0.27 cm^2/(V s) have also been reported for single crystals of hexathiapentacene (HTP) prepared by drop-casting a suspension of HTP nanowires on the prefabricated electrodes.[67]

3.3.2. Crystal Anisotropy. Because the intermolecular interactions in a crystal are anisotropic, the electronic transport will be strongly dependent on the measurement direction. Therefore, single-crystal devices are ideal to explore the intermolecular interactions/mobility relationships since the crystal packing and molecular orientation are clearly fixed. The example described before regarding rubrene single-crystal OFETs fabricated on a PDMS stamp, in addition to leading to very high performance devices, was also a pioneer work in the study of the field-effect mobility anisotropy.[78] The elastomeric stamp technique is nondestructive and reversible, so the contact between the stamp and organic crystals can be re-established many times without damaging the crystal or affecting the transistor characteristics. By measuring the crystal at different crystallographic directions in the *ab* plane, it was found that the crystal exhibited the maximum mobility along the *b* axis, which is the π stacking direction (Figure 13b). Using quantum-chemical calculations of the electronic band and vibrational reorganization energy, the marked anisotropy of the mobility related to the crystallographic axis of rubrene crystals has also been evaluated, and the results confirm that the cofacial π interactions give rise to very efficient electronic coupling, which is coincident with the experimental data.[83]

An improved method that consisted of a circular array of electrodes prefabricated on the PDMS substrate was also applied to measure rubrene single crystals. This design does not require the movement of the crystal and offers higher angle resolution (15°).[84]

Fan-shaped electrodes on Si/SiO_2 substrates have also been used to measure the anisotropic field-effect mobility in a free-standing single-crystal pentacene to which pressure was applied to enhance the contact.[85] More recently, the master equation coupled with the Marcus−Hush electron transfer theory has been applied to solve the charge carrier mobility in the pentacene *ab* plane. The anisotropic mobility of the hole carrier in this plane qualitatively agrees with the experimental result (Figure 15).[86]

Tetracene single crystals also show anisotropic transport in the *ab* plane, which is the herringbone plane, and the highest mobility is found along the [1, −1, 0] direction, which corresponds to the unit cell diagonal.[87]

The mobility anisotropy within a crystal was also tested by painting the electrodes with a conducting graphite paste or epoxy resin onto pregrown crystals of rubrene[88] and 4-hydroxycyanobenzene.[89] In the latter case, the crystals were grown from

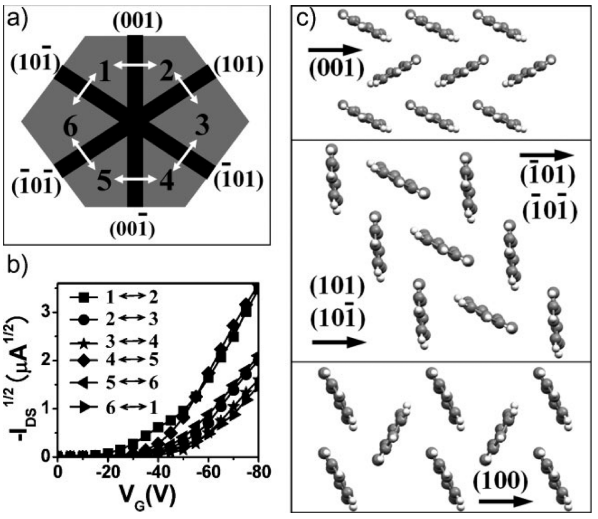

Figure 16. (a) Schematic diagram of the transistor of DBTDT with conduction channels parallel to the lateral crystal planes. (b) Transfer curves of different crystal planes. (c) The monolayer molecular arrangements along the (0,0,1), (1,0,1), (1,0,−1), (−1,0,1), (−1,0,−1), and (1,0,0) planes. Reprinted with permission from ref 94. Copyright 2009 Wiley-VCH Verlag GmbH & Co.

solution and the mobility along the third crystallographic direction was also investigated by space-charge-limited current measurements.

Recently, an anisotropic ambipolar behavior was observed in single-crystal OFETs of the semiconductor 2,5-bis(4-biphenylyl)bithiophene using a crossed gold wire as a shadow mask to deposit the electrodes. The devices showed different electron and hole mobilities depending on the crystal directions, the electron mobility being significantly more sensitive to the transport direction than the hole mobility.[90]

However, all the previous methods can only be applied to relatively large crystals to be able to manipulate or contact them. Bao and colleagues reported the investigation of the mobility anisotropy on randomly oriented small crystals (a few tens of micrometers) of dicyclohexyl-α-quaterthiophene grown in a solution and drop-cast onto a gold electrode array by measuring numerous crystals and plotting the dependence of the field-effect mobility on the crystal orientation.[91] Anisotropy in single-crystal transistors with channel lengths in the range of 1−20 μm of bis(phenylvinyl)anthracene (DPV-Ant), which has a herringbone structure similar to that of pentacene, has also been measured by employing the "organic ribbon mask" method.[92] The highest mobility of DPV-Ant single crystals was 4.3 cm^2/(V s) along the *a* axis, that is, the direction in which the molecular packing is denser, indicating stronger intermolecular interactions. The mobility anisotropy ratio μ_a/μ_b was 1.5−1.95.[93] This method was further developed by Li et al., who fabricated a 2D organic ribbon mask to probe the transport anisotropy of the dithiophene derivative dibenzo[*d*,*d*′]thieno[3,2-*b*;4,5-*b*′]-dithiophene (DBTDT), which showed a μ_c/μ_a ratio of around 2.0−2.5, consistent with the fact that in the *c* axis the molecular packing was closer (Figure 16).[94] A similar anisotropy ratio has been found in the excellent performing DNTT single crystal with a maximum mobility of 4 cm^2/(V s) along the *a* axis, which, according to calculations, is the one that shows the highest transfer integral values.[95]

Theoretical calculations of the transfer integral and reorganization energies of organic semiconductors have proved to be a very useful tool to design new promising materials or to rationalize a trend in mobilities within a series of molecules, but very importantly, calculations also offer a very powerful tool to predict the mobility anisotropy in organic semiconductors. Indeed, experiments and theory meet each other often since the best mobilities in single-crystal OFETs have been commonly found along the directions where the transfer integrals were maximum.

However, it should be kept in mind that experimental and calculated absolute mobility values might differ, since the theoretical ones are typically obtained considering exclusively the active organic materials, while the charge carrier mobilities found experimentally are, in fact, device mobilities since they also include all the effects of the device characteristics. In particular, contact resistances (i.e., charge injection barriers) can significantly reduce the device mobility.[96] Studies regarding the influence of the metals employed for the source−drain electrodes or the device architecture (e.g., top contact versus bottom contact) on the device mobilities have been carried out.[97] For instance, single-crystal OFETs based on the semiconductor hexamethylenetetrathiafulvalene (HM-TTF) exhibited an OFET mobility of 0.02 cm^2/(V s) when Au was employed as source−drain electrodes, but this value was improved to 10.4 cm^2/(V s) when the conducting organic charge transfer salt tetrathiafulvalenetetracyanoquinodimethane (TTF-TCNQ) was used due to optimized charge carrier injection.[98]

3.3.3. Patterning of Single Crystals. As mentioned before, organic single crystals offer a unique model to gain a deeper understanding of the interplay between the molecular interactions and the field-effect mobility. However, to use them for the fabrication of devices for industrial applications, it would be necessary to fabricate a large array of devices covering large areas. Recently, a few groups have devoted their efforts to the patterning of single crystals of organic semiconductors to prepare OFETs, that is, to controlling the specific location of the crystals on the substrate. One of the methodologies reported by Briseno et al.[99] was based on the patterning of an octadecyltriethoxysilane (OTS) film by microcontact printing on a substrate and then evaporating the organic material on the top. The rough topography in the stamped OTS domains served as nucleation points for the selective crystallization of the organic semiconductor. Nanocrystal seeds deposited on a substrate have also been employed as nucleation points for fabricating OFETs with copper phthalocyanine[100] and copper hexadecafluorophthalocyanine.[101] Finally, templates of certain self-assembled monolayers (SAMs) are also appropriate for growing selectively organic single crystals from solution since they can also function as nucleation sites[102] or can be used in (de)wetting patterning processes.[103] For a more extended review on patterning crystalline semiconductors, we recommend ref 104 to the reader.

3.4. Correlation of Crystal Structure with Mobility in TTF Derivatives

TTF derivatives are a suitable platform to perform structure−mobility correlation studies, due to the fact that their chemistry is very well-known, making it possible to synthesize a large variety of very similar molecules exhibiting different solid-state organizations. Their molecular packing is mainly determined by the $\pi-\pi$ stacking together with the S···S interactions of the TTF core. Moreover, often TTF derivatives are functionalized with sulfur-based heterocycles, which introduce further S···S and S···H−C interactions. A set of single-crystal OFETs using eight different TTF derivatives, which are shown in Figure 17, namely,

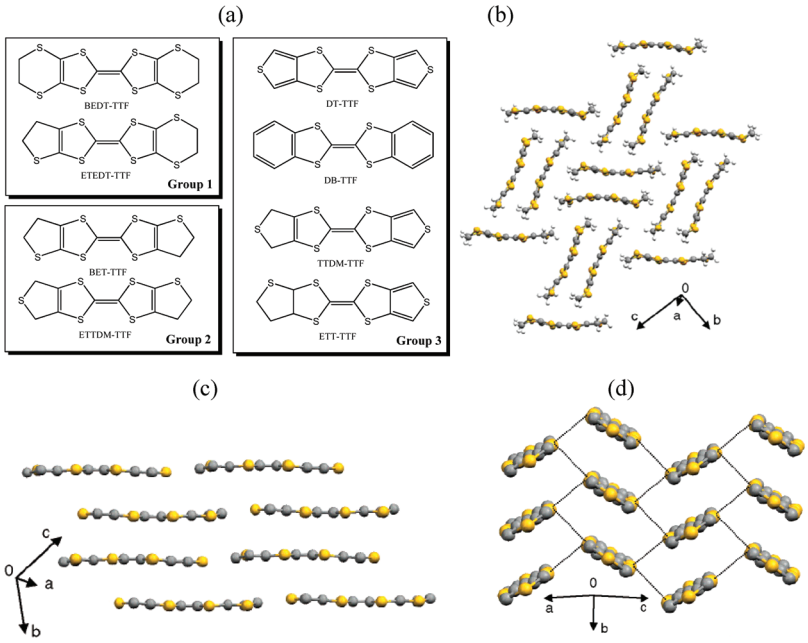

Figure 17. (a) Molecular structures of TTF derivatives for single-crystal OFETs. These molecules are classified into three groups according to their crystal packing. (b) Crystal structure of the dissymmetric ETEDT-TTF representative of group 1. (c) Crystal structure of the dissymmetric ETTDM-TTF representative of group 2. (c) Crystal structure of TTDM-TTF, one of the members of group 3 (S···S contacts as dotted lines). Hydrogen atoms have been omitted for clarity. Reprinted from ref 81b. Copyright 2004 American Chemical Society.

bis(ethylenedithio)tetrathiafulvalene (BEDT-TTF), (ethylenethio)(ethylenedithio)tetrathiafulvalene (ETEDT-TTF), bis(ethylenethio)tetrathiafulvalene (BET-TTF), (ethylenethio)(thiodimethylene)tetrathiafulvalene (ETTDM-TTF), dithiophenetetrathiafulvalene (DT-TTF), dibenzotetrathiafulavlene (DB-TTF), (thiophene)(thiodimethylene)tetrathiafulvalene (TTDM-TTF), and (ethylenethio)(thiophene)tetrathiafulvalene (ETT-TTF), were fabricated.[81] Thus, taking into account the crystal packing in which these molecules are arranged, this family of compounds could be classified into three groups. BEDT-TTF and ETEDT-TTF belong to the first group. Their supramolecular organization consists of dimers sustained by hydrogen bonds that form chains due to lateral S···S interactions. The chains are arranged perpendicularly to each other, therefore avoiding the formation of stacks. In the second crystal structure group, BET-TTF and ETTDM-TTF crystallize in a brickwork-type motif, forming chains of quasi planar molecules interacting side-by-side. These chains stack into layers, giving rise to a bidimensional electronic structure. Finally, the molecules from group 3, DT-TTF, DB-TTF, TTDM-TTF, and ETT-TTF, when crystallized form uniform cofacial π stacks of almost planar molecules with a short interplanar distance between molecules of one stack (3.56−3.66 Å) and short lateral S···S interactions between molecules of different stacks (3.55−3.72 Å). A clear correlation between crystal structure and device performance was found as a notable improvement of the charge carrier mobility was observed on going from group 1 to group 3. It is also worth noting that the symmetric TTFs exhibited higher mobility than the corresponding dissymmetric derivatives, probably due to the higher disorder that the latter present on their crystals. This trend was also in agreement with the theoretical calculations; that is, the materials showing higher mobility have a lower reorganization energy and larger transfer integral as Marcus theory predicts for hopping transport.[81]

We should also mention that, in the single-crystal OFETs reported by Saito and colleagues, with hexamethylene-TTF, which crystallizes following a brickwork fashion similar to that of BET-TTF, high mobilities (0.02 $cm^2/(V\ s)$ using gold electrodes) on the order of those obtained with the molecules belonging to group 2 from the previous investigation were also achieved.[98]

Mori et al.[105] also investigated a family of phenyl-substituted TTF derivatives that when crystallized form modified herringbone-type structures. The molecular long-axis projections of these structures were almost the same, but the crystal structures differed in the displacements of the molecules perpendicularly to this layer. They observed that when this shifting of the molecules provoked the restriction of the intermolecular interaction in one dimension, the OFET mobility was drastically reduced.

In conclusion, the chemical modification of the building blocks to prepare organic semiconductor materials can, in principle, be a very suitable strategy to tune their solid-state structure and, consequently, their transport properties. However, in practice, the prediction of the crystal structures of the modified molecules is not straightforward at all: small variations in the molecular structure can lead to completely different solid-state structures. Even the changes in the experimental procedures followed to crystallize one unique material can result in the formation of different polymorphs (see the section "Polymorphism"), adding further complexity to this issue.

4. POLYMORPHISM

It is well-known that, owing to the weak interaction energies, organic molecules are prone to polymorphic formation in the solid state. This results in different crystal structures with comparable intermolecular interactions, which can be greatly affected by the crystallization conditions.[106,107] Most organic

semiconductors can therefore crystallize in a variety of polymorphs that can yield different device performances, and consequently, the study and control of polymorphism is very important in this field. Various studies on polymorphism from the point of view of preparation methods of thin films and crystals as well as crystal packing and polymorphic transformations of the most representative organic semiconductor have been published. However, reports on the OFET performance of the different polymorphic modifications of a certain semiconductor are still scarce.[108−111]

4.1. Pentacene and Related Acenes

The first triclinic crystalline structure of pentacene was reported in 1961.[112] Nevertheless, subsequent structure determinations in single crystals grown by different techniques have never reproduced this first structure but different triclinic ones, all of them with a herringbone-type packing of pentacene molecules.[113] Only recently, Brillante et al.[114,115] reported that vapor growth at 500 K under an inert atmosphere yields tiny microcrystals that were identified as the same polymorph, phase C, by powder X-ray diffraction. The authors have studied by lattice phonon Raman confocal spectroscopy, a very powerful tool for the study of polymorphism,[116] the differences in polymorphs C and H and have demonstrated that, in many of the powders studied, there are phase inhomogeneities by diffusion of one polymorph inside the other. This technique was also employed to investigate pressure experiments, revealing that crystals of polymorph C irreversibly transform into the denser H polymorph at elevated pressures.[115] These two phases represent the deepest energy minima in energy minimization of pentacene using quasi-Monte Carlo sampling; that is, they are the most stable forms of pentacene.[117]

The effect of temperature on polymorphic transformation of pentacene crystalline powders of phase H grown by horizontal physical vapor-phase transport have also been explored.[118] It has been observed that when the crystals of this phase, also named the "low-temperature (LT) phase", are heated, an incomplete phase transformation to a new polymorph starting at around 463 K takes place. This polymorph, named the "high-temperature (HT) phase",[119] has a larger d spacing (14.5 Å) and remains stable on lowering the temperature. The pentacene-HT unit cell is consistent with the unit cell first reported by Campbell et al.[112] and corresponds to phase C. This transformation is first order, as evidenced by the coexistence of two phases over a broad temperature range from powder diffraction. Both structures are very similar with a herringbone-type packing. The herringbone-type layers are virtually identical, but the polymorphs differ in the shift between adjacent layers. Figure 18 shows both polymorphs superimposed, illustrating the relative molecular displacements.

The polymorphism of pentacene has also been widely investigated for thin films and rationalized theoretically.[120] In thin films, at least four different polymorphic modifications of pentacene have been identified so far, which are characterized by interplanar d_{001} spacings of 14.1, 14.5, 15.1, and 15.4 Å. Nevertheless, mainly two of these polymorphs are found by the vacuum deposition process: the one with a 14.5 Å d_{001} spacing, which corresponds to the bulk HT phase, and the one with a 15.4 Å d_{001} spacing, which is named the "thin-film phase" because it is commonly found in the first stages of film growth. The appearance of polymorphs depends on the growth conditions, such as the substrate, temperature, or film thickness.[166b−121] A clear thickness dependence of polymorphs is found when they are grown on SiO_2. Ultrathin films have the same lattice constants as

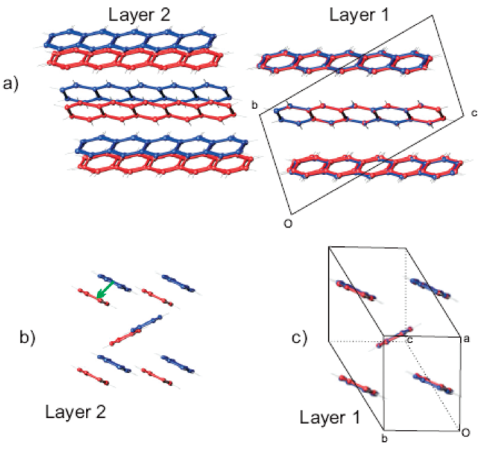

Figure 18. Crystal structure of the two pentacene polymorphs superimposed (blue, low-temperature (pentacene-LT) phase; red, high-temperature (pentacene-HT) phase). In (a), the layered type of the herringbone structure is illustrated. Layer 1 and layer 2 (its adjacent layer) are isolated and drawn in a different orientation in (b) and (c), respectively. The arrow in (b) indicates how the layers are shifted in the two different crystal structures. Reprinted with permission from ref 118a. Copyright 2007 Wiley-VCH Verlag GmbH & Co.

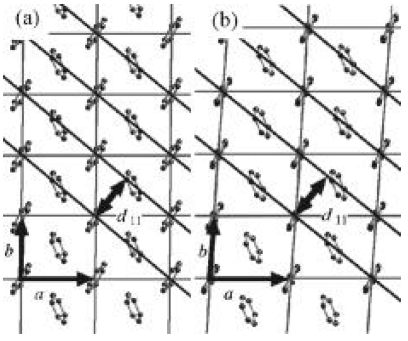

Figure 19. Schematic illustration of the *ab* plane with the lattice spacing d_{11} of the polymorphs: (a) thin-film phase and (b) bulk phase. Reprinted with permission from ref 122. Copyright 2007 American Institute of Physics.

those of films around 100 nm thick when a polymorphic transformation to the bulk phase occurs.[122] Figure 19 shows an illustration of the two phases with the lattice spacing d_{11} of the polymorphs differing by 2 Å. When the gate dielectrics used are SAMs of different lengths, it has been found that, at the first stages of the film growth (until 60 nm), depending on the alkyl chain length, the pentacene monolayers in contact with the SAM could adopt both competing crystalline phases ("thin-film" phase and "bulk phase"), which affected the π-conjugated nanostructures in the ultrathin and subsequently thick films.[123]

Tetracene (TC) polymorphs have been studied for more than 30 years. The structure of the first polymorph has been known since 1962 and belongs to the triclinic structure commonly named the "HT polymorph".[124] This polymorph undergoes phase transitions produced by lowering the temperature and increasing the pressure as observed by different authors employing several techniques.[125−129] The same polymorph is obtained by both external stimuli. The crystal parameters of the LT phase have been determined, and a structure has been proposed on the

dx.doi.org/10.1021/cr100142w |*Chem. Rev.* 2011, 111, 4833–4856

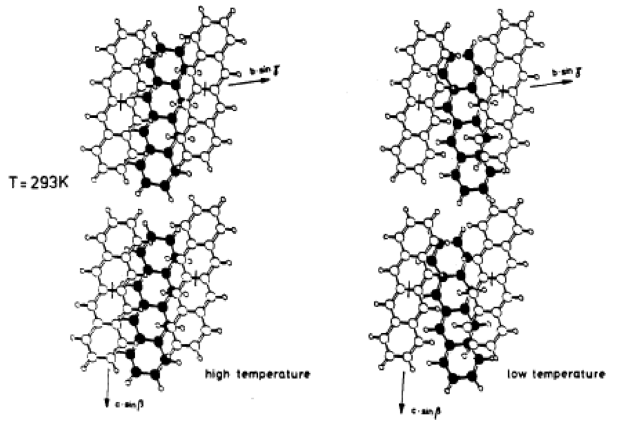

Figure 20. Arrangement of TC molecules viewed along the [1,0,0] direction of the HT and LT structures. Reprinted with permission from ref 127. Copyright 1985 Chemical Physical Society.

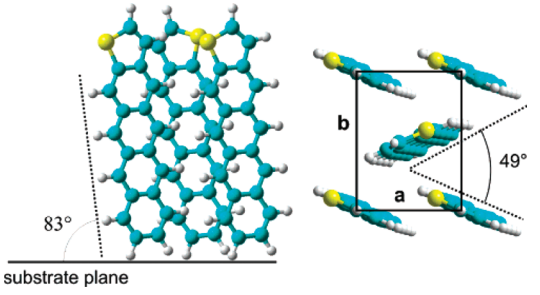

Figure 21. Thin-film structure of tetraceno[2,3-*b*]thiophene as predicted by the packing calculations, representing the lowest energy configuration of two thiotetracene molecules in a unit cell. Reprinted from ref 130. Copyright 2008 American Chemical Society.

basis of lattice energy calculations (Figure 20). This second polymorph is only stable at low temperature (below 140 K) or high pressure (well above 1 GPa), and reversible changes have been observed by lattice phonon Raman spectroscopy. As observed with pentacene, this denser polymorph that is metastable can also be prepared by sublimation in an inert atmosphere at reduced pressure[126] and is maintained at ambient pressure and temperature.

As in the case of pentacene, a thin-film phase and a bulk phase have been detected for tetraceno[2,3-*b*]thiophene, in which a terminal benzene ring of pentacene is replaced by a thiophene ring. A single triclinic phase (thin-film phase) exists in all samples with less than 20 nm thickness (Figure 21).[130] This thin-film structure is different from that reported for the bulk crystal structure, which is orthorhombic.[131] Both of them nevertheless present a herringbone packing as in all phases of pentacene. Figure 22 shows the crystal structure of the bulk phase in comparison with that of pentacene. The fact that the differences in both structures are small is reflected in the very similar performances of OFETs prepared with films of 20 nm thickness (thin-film phase)[130] and 50 nm thickness formed by a single-crystalline phase (bulk phase), which has shown mobilites as high as 0.47 $cm^2/(V\ s)$.[132]

Several polymorphs of rubrene have been reported, although not for all of them have the complete atomic coordinates been published.[133] The high-mobility OFETs reported based on crystals of rubrene obtained from the vapor phase have been

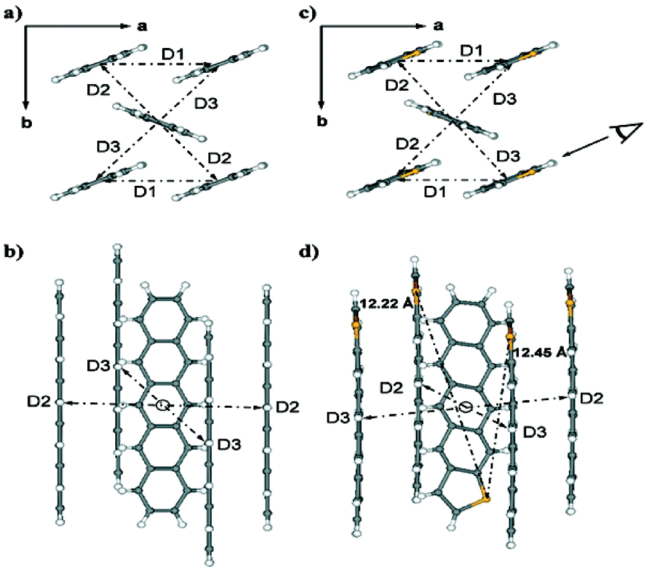

Figure 22. View of the *ab* layer of (a) pentacene and (c) tetraceno[2,3-*b*]thiophene and side view of the packing of (b) pentacene and (d) tetraceno[2,3-*b*]thiophene. Reprinted from ref 131. Copyright 2007 American Chemical Society.

attributed to an orthorhombic phase.[78] However, a monoclinic and a triclinic phase were also previously identified over 50 years ago.[133c,d] More recently, microcrystals ranging from 1D ribbons to 2D rhombic and hexagonal plates have also been prepared employing the reprecipitation method depending on the monomer concentration.[134] The 1D ribbons have been identified to correspond to a triclinic phase and the 2D plates to a monoclinic one. In parallel, Matsukawa et al. have prepared rubrene single crystals from 1-propanol solutions.[111] Hexagonal crystals from the orthorhombic phase were obtained together with parallelogram-shaped crystals from a triclinic phase, the crystal parameters of which seem to be in agreement with those of the crystals obtained by the previous method. Interestingly, OFETs were here prepared with both polymorphs, obtaining a mobility 1 order of magnitude higher for the orthorhombic phase (up to 1.6 $cm^2/(V\ s)$).

An especially appealing study has very recently been carried out by Jurchescu et al. regarding a phase transition between two polymorphs of fluorinated 5,11-bis((triethylsilyl)ethynyl) anthradithiophene (diF-TES-ADT) with temperature in both single-crystal and thin-film OFETs.[109] Despite the fact that neither the crystal structure nor the electrical properties change dramatically, since the transition occurs near room temperature, this work sheds light on how polymorphism can affect the long-term performance of the devices. Figure 23 shows the evolution of the transition from the LT polymorph to the HT one in a thin film of diF-TES-ADT followed by checking the position of the (0,0,1) peak in the X-ray diffraction data. As can be seen in the figure, the OFET mobility increased when the HT polymorph was being formed whereas the activation energy (i.e., extracted from the slope in the μ vs T graph) decreased.

Another polyaromatic semiconductor, diindenoperylene (DIP), also presents an enantiotropic polymorphic phase transformation at 403 K, and both phases have been chacterized by single-crystal X-ray diffraction.[135] Both the triclinic LT α-phase and the monoclinic HT β-phase have a herringbone-type structure. The epitactic transformation from the α-phase to

dx.doi.org/10.1021/cr100142w |*Chem. Rev.* 2011, 111, 4833–4856

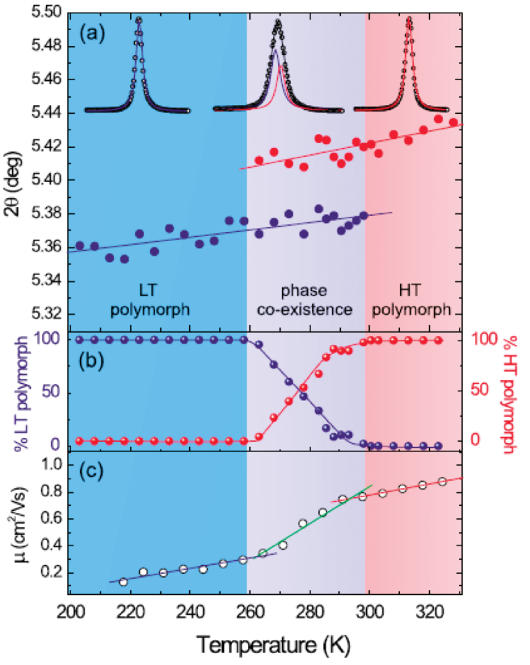

Figure 23. (a) Evolution of the (0,0,1) peak position for the LT polymorph (blue) and HT polymorph (red). The insets represent typical peak fits. (b) Evolution of the concentration of the LT polymorph (blue) and HT polymorph (red). The phase coexistence region can be observed. (c) Evolution of the diF-TES-ADT thin-film transistor field-effect mobility with temperature. Reprinted with permission from ref 109. Copyright 2009 American Physical Society.

the β-phase involves strong shearing displacements as well as bending and torsional deformations of the DIP molecules (Figure 24). In thin films grown on SiO_x the pure HT phase is formed.[136]

Remarkably, this compound shows both hole and electron transport as ascertained by time of flight measurements. The temperature-dependent mobility behavior indicates the effect of the structural phase transition being higher in the case of electron transport, which shows a big drop of mobility above 400 K.[137]

4.2. Oligothiophenes

Unsubstituted oligothiophenes (nTs) crystallize in the same monoclinic space group in $P2_1/a$, $P2_1/c$, or $P2_1/n$ alternative cell choices and present herringbone-type packing. However, the number of molecules per unit cell (Z) may be either 2 or 4. Bithiophene[138] belongs to the first group, whereas 5T[139] and 8T belong to the second one. So far, only for 4T and 6T, two polymorphs corresponding to both forms have been found.

The two polymorphs of α-quaterthiophene show different backbone arrangements, although both of them give rise to a herringbone-type packing (Figure 25).[139−141] Single crystals grown from the vapor phase at a source temperature of 140 °C belong to the LT phase, whereas those grown at source temperatures of 160, 180, or 200 °C or from the melt are of the HT phase. When the temperature is raised above 200 °C and crystals are left to grow with no external cooling, polycrystalline samples composed of a mixture of the two phases appear, as observed by confocal Raman mapping.[142] The two polymorphic forms can also be distinguished by using different techniques such as inelastic neutron scattering,[143] infrared spectroscopy,[144] or polarized Raman spectroscopy,[142] among others. Additionally, an irreversible solid−solid phase transition from the LT to the HT

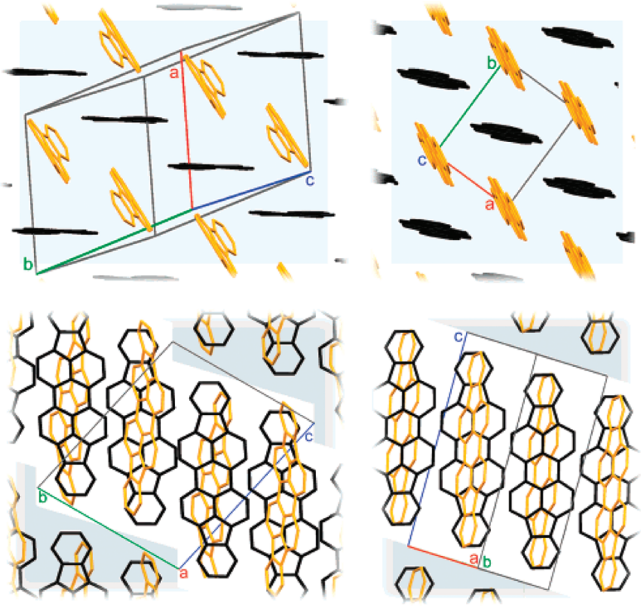

Figure 24. Herringbone layers of the α-phase (left) and the β-phase (right). The twist and bend in the DIP molecules in the α-phase are clearly visible. The larger tilt away from the c^* axis in the α-phase is reflected in the unit cell indicated. In the lower part, the herringbone layers are depicted from the side, showing the alignment of the rows of molecules. Reprinted from ref 135. Copyright 2007 American Chemical Society.

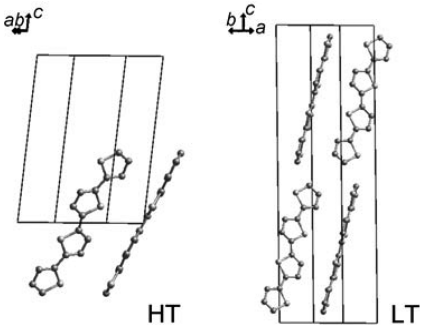

Figure 25. Quaterthiophene: HT ($P2_1/a$, $Z = 2$) and LT ($P2_1/c$, $Z = 4$) crystal structures. Reprinted with permission from ref 142. Copyright 2009 Wiley-VCH Verlag GmbH & Co.

polymorph (4T/LT to 4T/HT) at 191 °C has recently been reported which permits preparation of large and thick HT single crystals, preserving the overall crystallinity of the starting LT single crystals grown by the floating-drop technique.[145]

Concerning α-sexithiophene (6T), similar polymorphism has been observed. Two polymorphs have also been identified in bulk crystals, the LT phase with $Z = 4$[146] and the HT phase with $Z = 2$.[147] Different polymorphs are shown in Figure 26 together with their fingerprint in lattice phonon Raman spectra.[116] Both polymorphs have the molecules in a herringbone-type packing but with dissimilar π stacking. Whereas the slip of the molecules along the short molecular axis is very similar, the one along the long molecular axis differs significantly.[60]

The two 6T polymorphs can be obtained simultaneously from the same sublimation process, yielding mixed domains of the two phases, which show up as a physical impurity of one polymorph inside the other, without any morphological difference.[148]

dx.doi.org/10.1021/cr100142w |Chem. Rev. 2011, 111, 4833–4856

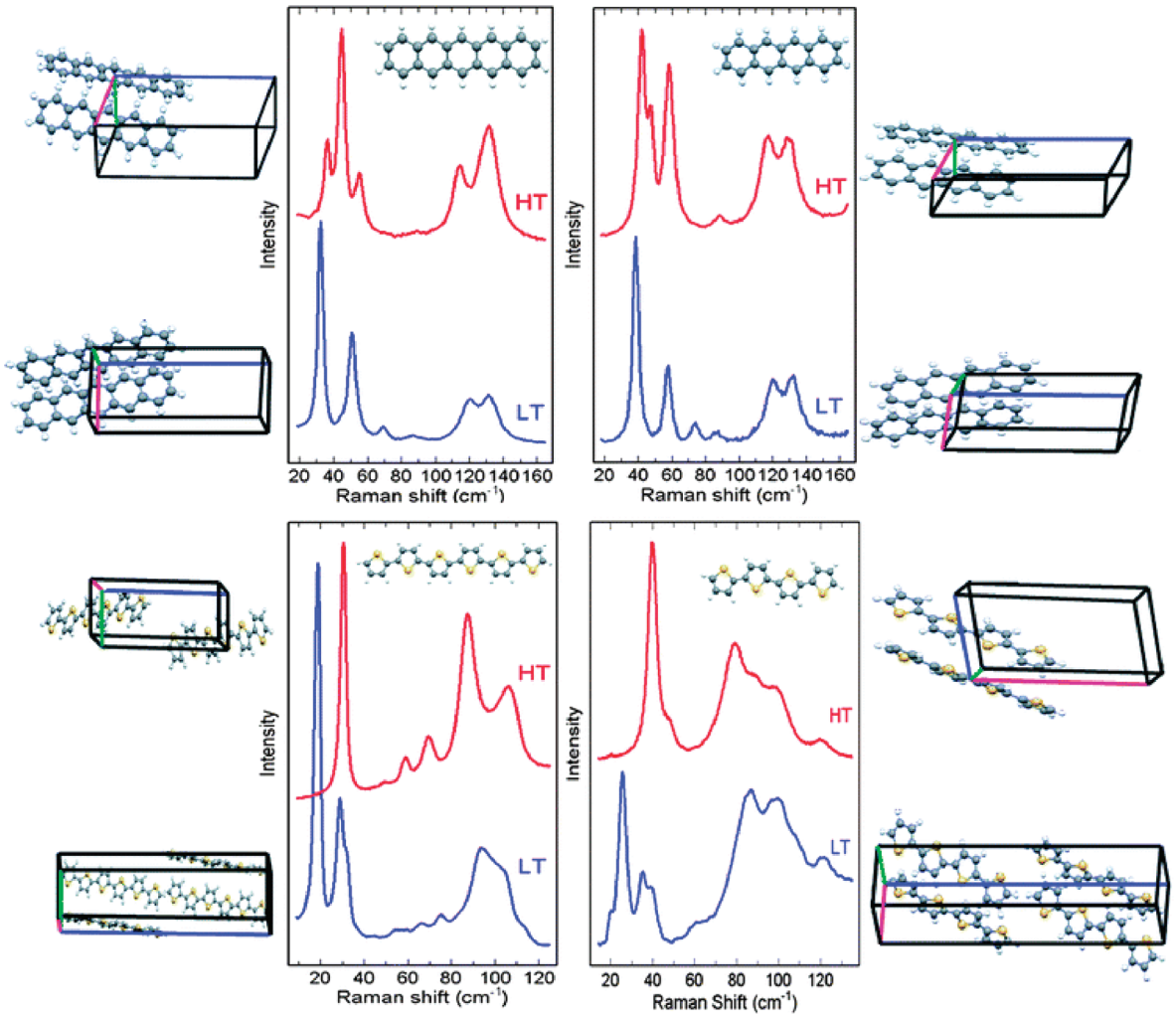

Figure 26. Crystal structure and the corresponding lattice phonon Raman spectra of the two polymorphic forms of α-sexithiophene. Reprinted with permission from ref 116. Copyright 2008 The Royal Society of Chemistry.

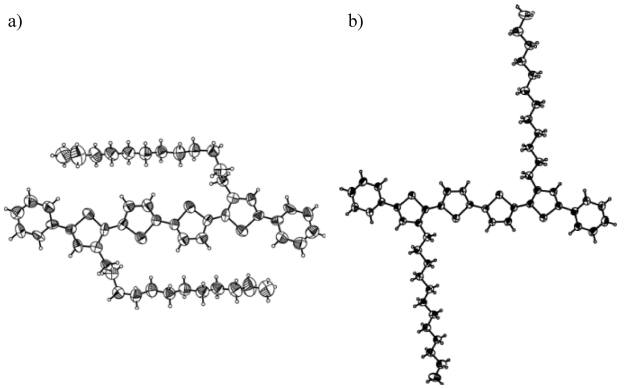

Figure 27. Thermal ellipsoid plots (prepared at the 30% probability level) of single-crystal molecular structures of 3,3‴-phenylquarterthiophene crystallized from (a) 2-propanol and (b) hexane. Reprinted with permission from ref 151. Copyright 2007 Wiley-VCH Verlag GmbH & Co.

Concerning growth as thin films, when the substrate is silicon oxide, "in situ" growth that shows that 6T grows as a unique crystalline layer from the beginning of the evaporation has been studied. The thin-film phase corresponds to the LT polymorph and is the same as the bulk phase that occurs above 5−6 monolayers.[149,150] Thin films grown on mica also yield the LT phase.

When the oligothiophenes are substituted, the polymorphism can arise not only from the backbone organization but also from pendant side chain conformational changes. In this respect a family of 3,3‴- didodecylquarterthiophenes present a unique yet general polymorphism associated with side chain conformational arrangements.[151] Those with long backbone structures due to phenyl substituents show two different side chain conformationally induced polymorphs, one with a fully extended side chain and one with a bent side chain conformation (Figure 27). Different polymorphs are obtained by crystallization in different solvents. Good solvents (hexane, toluene, dichloromethane) promote polymorphs with fully extended dodecyl side chain conformations, whereas poorer solvents, such as as propanol, promote polymorphs with the bent chain conformation.

The polymorphism in molecular structures gives rise to different packings. In polymorphs with fully extended chains, the packing is herringbone type with interdigitated chains, and in polymorphs with bent chains, an almost complete slipped herringbone packing is observed. The same polymorphism was also manifested in thin

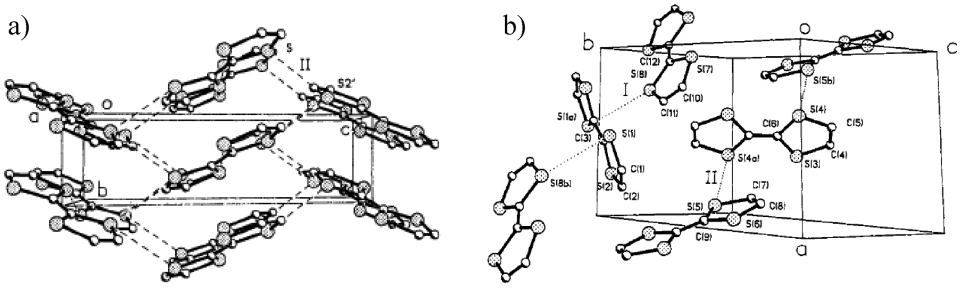

Figure 28. (a) View of the *bc* plane of the crystal structure of α-TTF. (b) Partial view of the crystal structure of *β*-TTF, showing the relationships among the four different molecules in the unit cell (each lying on the inversion center) and the formation of chains. Reprinted from ref 153. Copyright 1994 American Chemical Society.

films. Thin films prepared by dip-coating a solution of these compounds in propanol gives a diffraction pattern corresponding to the polymorph with bent side chains, whereas when hexane or toluene was used as the solvent, a mixing of polymorphs with extended and bent side chains was obtained.[151]

4.3. Tetrathiafulvalenes

The simplest member of this family of compounds, TTF, exists in two polymorphic modifications. The single-crystal structure determination of α-TTF was described in 1971,[152] and 20 years after, one brown crystal of the second phase was obtained by serendipity in the course of preparing tellurium derivatives of TTF.[153] As clearly observed in Figure 28 the two crystal structures are quite different. Thus, whereas the α-phase has a herringbone-type structure and a short *b* axis leading to a strong π stacking along this direction, the *β*-phase can be described as zigzag chains sustained by S···S interactions. The α-phase also has many interchain short S···S interactions leading to the 2D network shown in Figure 28a.

Recently, the two phases have been selectively prepared by crystallization on OTS-modified substrates by using different solvents.[110] Crystals of the pure α-phase were obtained from *n*-heptane or *n*-hexane,[154] whereas from chlorobenzene the pure *β*-phase was produced. This *β*-phase is also exclusively produced by vapor-phase growth under a mild vacuum (∼1 mbar).[154]

OFETs based on single crystals of both phases demonstrated that the maximum mobility of the α-phase was near 1.20 $cm^2/(V\,s)$, while *β*-phase crystals exhibited a mobility about 1 order of magnitude lower, reaching a maximum value of 0.23 $cm^2/(V\,s)$.[110] The better performance of α-phase crystals was explained by the strong contribution of the $\pi-\pi$ as well as S···S intermolecular interactions.

Polymorphism has also been studied for crystals and thin films of DB-TTF grown with different methodologies.[155] Despite being a simple molecule, DB-TTF has a very complex polymorphic behavior. This organic semiconductor presents, at ambient conditions, four polymorphic modifications. In addition to the first known monoclinic structure (α) with $Z = 2$ (Figure 29a),[105,156] two other crystal structures have been resolved: *β*, also monoclinic, but with $Z = 4$ (Figure 29b), and *δ*, a triclinic polymorph (Figure 29c).[155,157] An additional polymorphic modification (γ) has been identified by means of lattice phonon confocal Raman microscopy and XRD.

In the α-phase, almost planar molecules of DB-TTF stack along the *b* axis with an interplanar distance of 3.545 Å, forming a herringbone arrangement with an angle of 52.64°. The crystal structure of the *β*-phase shows less planar molecules with a herringbone packing motif in which molecules have more or less

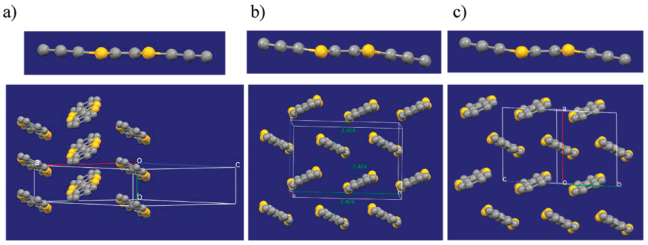

Figure 29. View of one molecule of DB-TTF along the shortest dimension and of the crystal packing motif of the (a) α-phase, (b) *β*-phase, and (c) *δ*-phase. Sulfur atoms are identified by the yellow color.

edge-to-face packing with an angle of 52.22° between the mean planes of molecules. In contrast to the α phase there is no $\pi-\pi$ overlap between consecutive molecules in the stacks along *b*. The molecules form a zigzag chain along the *c* axis with short contacts of 3.464 Å between sulfur atoms of one molecule and the central carbon atom of the next molecules in the chain. There are no short contacts between adjacent chains, which are therefore isolated, in contrast with the α-phase in which interstack S···S contacts are found. In the triclinic *δ*-phase, the molecules have a chairlike form with molecular geometries similar to that in the *β*-phase. The packing structure in this phase is a herringbone type with a tilt angle of 51.11°, which is also similar to that of the *β*-phase. However, the long axis is sliding, the number of intermolecular short contacts between the molecules is increased, and the contact distances are shorter compared to those of the α- and *β*-phases.

Physically pure α-phase was obtained by crystallization of DB-TTF at room temperature from hot chlorobenzene and DMF solutions, as well as by drop-casting on Si/SiO_x from hot chlorobenzene. Single crystals of the *β*-phase were prepared by recrystallization from a saturated solution in hot toluene. They were always obtained mixed with single crystals of the α-phase. However, both phases could be easily identified by their peculiar morphologies: well-shaped needles and small prisms, corresponding to the pure α- and *β*-phases, respectively. Pure γ-phase has been identified in polycrystalline films obtained both by ultra-high-vacuum (UHV) vapor deposition on SiO_x substrates at temperatures of 50 and 70 °C and by drop-casting a colloidal composite of polystyrene (PS) beads and DB-TTF in different solvents. The fourth polymorph, the *δ*-phase, was obtained physically pure by crystallization from a 1:1 mixture of 2-propanol:nitromethane as well as by vapor deposition under a vacuum (10^{-2} Torr, 190 °C). Very recently this polymorph was also obtained as a single crystal by vapor transport.[157] Lattice phonon

dx.doi.org/10.1021/cr100142w |*Chem. Rev.* 2011, 111, 4833–4856

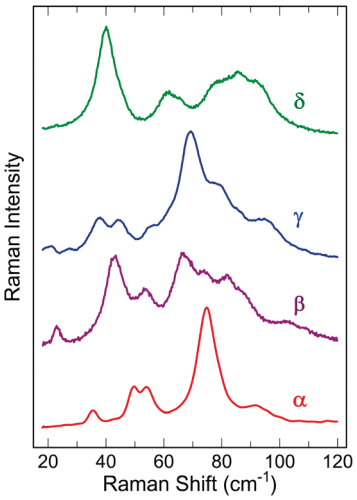

Figure 30. Lattice phonon Raman spectra of the four polymorphic forms of crystalline DB-TTF. Reprinted with permission from ref 155. Copyright 2008 The Royal Society of Chemistry.

confocal Raman microscopy permits easy identification of the four polymorphic forms of crystalline DB-TTF as clearly seen in Figure 30.

The γ-phase is the favorite one in fast evaporation processes; thus, it may be the one that is kinetically dominant. This phase is typical of a film, with strong interaction with the surface, but cannot be obtained as a bulk phase. A typical experiment of vapor deposition on a cold tip starts with the initial deposition of the pure γ-phase as a film. By further increasing the amount of sublimed material on the top of the microcrystalline film like layer, some larger needle-shaped crystals of the α-polymorph start to grow as a bulk phase.

This scenario, involving so many polymorphs and often phase mixing for DB-TTF, is due to the fact that the solubility of TTF derivatives permits them to be processed not only by the classic vacuum deposition of thin films but also by several kinds of crystal growth techniques from solution, with a large variety of solvents. It is well-known that the number of polymorphs found for a specific molecule is directly related to the number of different experiments performed to grow crystals.[106]

OFETs based on single crystals of the α-phase prepared by drop-casting a chlorobenzene solution gave a charge mobility μ as high as 1 $cm^2/(V\ s)$,[81d] whereas in devices based on vacuum-sublimed thin films, which should contain either pure γ-phase or a mixture of phases, μ ranged from 0.012 to 0.06 $cm^2/(V\ s)$.[105,158]

The high-mobility TTF derivative DT-TTF has also been recently shown to give rise to two polymorphs. Long plate crystals of DT-TTF, namely, the α-phase, can be easily prepared from a solution employing a variety of solvents.[159] As mentioned in a previous section, these crystals belong to the monoclinic system, space group $P2_1/a$, with two centrosymmetric molecules per unit cell. The molecules form π stacks following a herringbone structure with the long axis tilted almost 20° to the c axis and facing along b, where the $\pi-\pi$ interactions are maximized. However, when DT-TTF crystallizes on surfaces (i.e., SiO_2 or parylene C) from a solution of toluene or dichlorobenzene, crystals showing thin hexagonal-shaped platelets coexist with the clearly identified crystals of the α-phase.[108] Polarized Raman spectra together with X-ray characterization revealed that the

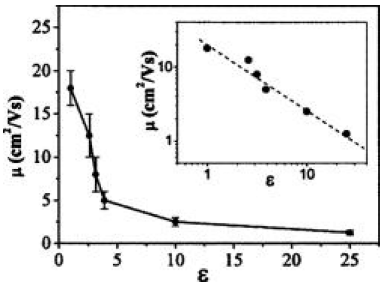

Figure 31. Decrease of the mobility with increasing ε as observed in rubrene single-crystal OFETs employing different gate insulators. Reprinted with permission from ref 161. Copyright 2004 American Institute of Physics.

β-phase crystallizes in a centrosymmetric monoclinic group (space group C_{2h}^5) with two molecules per unit cell, like the α-polymorph. The phases organize very similarly, though in the α-phase the molecules are slightly closer. Interestingly, both polymorphs were also prepared as thin films. However, while films of β-DT-TTF were obtained by evaporation on Si/SiO_2, films of α-DT-TTF were realized by the solution-processed technique of zone-casting.[45b]

In this case, thin-film and single-crystal OFETs were fabricated for both polymorphs and also employing different device configurations to inspect unequivocally the influence of polymorphism on the device performance.[108] Noteworthy, all α-DT-TTF OFETs exhibited higher mobility than the β-DT-TTF OFETs (from 2-fold to up to 1 order of magnitude higher), which was in agreement with the crystallographic data that indicated larger distances between neighboring molecules in β-DT-TTF.

Considering all the above discussion, it is clear that polymorphism can be a very complex issue. However, if organic devices are going to be implemented for commercial use, it will be imperative to be aware of the control of polymorphism in organic semiconductors, and therefore, this topic needs to be further explored.

5. INFLUENCE OF THE INTERFACES

As already mentioned earlier, the organic semiconductor/metal interface and especially the organic semiconductor/dielectric interface have a strong influence on the molecular order.

5.1. Organic Semiconductor/Dielectric Interface

The most widely used dielectric in OFETs has been SiO_2 grown on doped Si gates following the same technologies as the ones established for inorganic microelectronics. Nonetheless, in the past few years, there has been a lot of work on studying the influence on the OFET performance of different types of inorganic dielectrics as well as organic dielectrics compatible with solution processability, flexible substrates, and low-temperature processes.[4,160]

As an example, single-crystal rubrene OFETs have been fabricated using different materials as the gate insulator. It was observed that the mobility of the charge carriers systematically decreases with increasing dielectric constant of the gate insulator (Figure 31).[161] The authors explained that the effect is due to the fact that a (nearly) localized charge carrier at the rubrene/dielectric interface locally polarizes the dielectric. The electrostatic potential generated by the induced polarization exerts an attractive force on the charge carrier itself that increases the tendency toward carrier self-trapping. As the attractive force is

dx.doi.org/10.1021/cr100142w |Chem. Rev. 2011, 111, 4833–4856

larger for larger ε, this qualitatively explains why the mobility is reduced with increasing ε.

Furthermore, theoretical studies of the effect of polymeric dielectrics on pentacene have shown that the electrostatic interactions introduce a significant energetic disorder in the pentacene layer in contact with the polymer chains. A drop in the hole mobility by a factor of 5 is predicted with PS chains, while a drop of a factor of 60 is obtained for PMMA due to the presence of polar carbonyl groups.[162]

The characteristics of the dielectric can also be modified with surface treatments, such as growing SAMs. It has been demonstrated that these treatments often have strong effects on the film structure and on the resulting electrical characteristics.[163] As an example, we cite the work of Kelly et al., which achieved a very high OFET mobility (~3 $cm^2/(V\ s)$) for a pentacene thin film deposited on a 1-phosphonohexadecane-treated alumina dielectric.[164]

The vital importance of the interfaces is ascribed to the fact that the current transport in an OFET is known to take place in the first few molecular monolayers. In this direction, a few works have focused on the crystal structure characterization of the first (sub)monolayers of organic semiconductors such as 6T[165] and pentacene films on (treated) SiO_2. In the case of thin films of vacuum-sublimed pentacene, it was found that the structure of the first monolayer, which is influenced by the crystal structure of the first submonolayer, differs from that of the bulk material.[166] Very recently it has been demonstrated that the number of active layers in pentacene OFETs contributing to the current and the spatial distribution of charge carriers are modulated by the growth mode. The work shows that the effective Debye length is not just a material parameter, but depends on the multiscale morphology.[167]

Additionally, the monolayer by monolayer growth of thin films of 6T on the gate dielectric demonstrated that the first two monolayers next to the dielectric interface dominate the final OFET charge transport.[168] The solution-based technique of dip-coating has also permitted a controllable growth of aligned monolayer and multilayer stripes of the organic semiconductor DTBDT-C9 (Figure 5) by varying the pulling speed.[169] No OFET effect was observed in monolayer stripes due to their amorphous character, while good OFET bahavior has found in multilayer ($N \geq 2$) stripes.

Obviously, in all the cases, due to the high mobility anisotropy that organic semiconductors reveal, to achieve high mobility, it is imperative that the π overlap direction is parallel to the OFET channel, that is, parallel to the substrate, since if the molecules lie flat to the dielectric surface, very low mobility will be expected. This was observed for the perylene derivatives PTCDA and PTCDI-C8 (Figure 5): the poor transport of the former was attributed to the molecules stacking almost parallel to the substrate, while the latter packs inclined to the substrate and has shown an electron mobility of up to 0.6 $cm^2/(V\ s)$.[2c,170]

Taking into account the two previously mentioned aspects (i.e., in an OFET the conducting channel is formed just in the first molecular monolayers and the molecules at the interface should be arranged in a way that the direction where the electronic overlap is maximized is parallel to the substrate), Nuckolls and colleagues put forth a new strategy based on using organic semiconductors functionalized to spontaneously form upright monolayers directly linked to the gate oxides.[171] These monolayers could constitute the active layer in nanoscale OFETs, known as self-assembled monolayer field-effect transistors (SAMFETs). In this work, tetracene was functionalized with

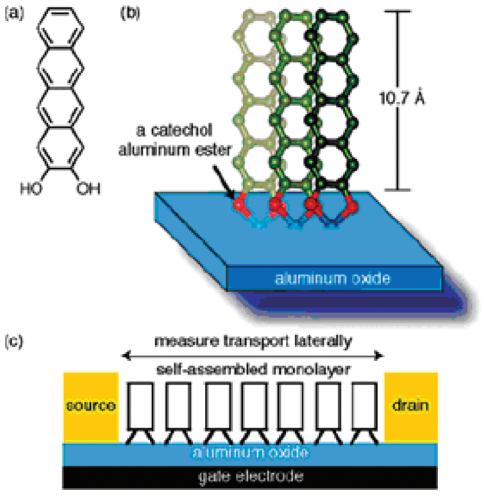

Figure 32. (a) Hydroxyl-functionalized tetracene. (b) Schematic of bonding and orientation of the functionalized tetracene on aluminum oxide. (c) Schematic of the self-assembled monolayer transistor. Reprinted from ref 171. Copyright 2004 American Chemical Society.

hydroxyl groups since they can chelate a variety of metal oxides via a mononuclear bidentate coordination. This allowed for the formation of a SAM on the aluminum oxide dielectric in a prefabricated OFET (Figure 32). Albeit it had no ideal transistor characteristics, the SAM behaved as a p-type semiconductor. The yield of the devices was relatively high for devices with channel lengths of 60 nm or shorter, but dropped off sharply for larger devices.

This approach regarding the preparation of nanoscale SAMFETs later proceeded in a similar way but employing as the organic semiconductors hexabenzocoronene[172] and oligothiophenes linked with a short alky chain.[173] In both cases, OFET behavior could be observed offering well-defined curves with a clear saturation, and in the latter case, a mobility on the order of 3×10^{-3} to 8×10^{-4} $cm^2/(V\ s)$ was extracted.

More recently, SAMFETs with channel lengths and a width of up to 40 and 1000 μm, respectively, exhibiting bulklike carrier mobility (up to 0.04 $cm^2/(V\ s)$), large current modulation, and high reproducibility were reported employing liquid-crystalline molecules consisting of a π-conjugated oligothiophene mesogenic core separated by a long aliphatic chain from the anchoring group.[174] In addition, SAMFETs were combined into logic gates as inverters as a first step toward functional circuits. Employing the same system, dual-gate transistors have also been found.[175]

Heteropitaxy growth represents a completely different strategy to induce crystallinity in thin films. Polycrystalline films of the high-performing semiconductor rubrene have been prepared by growing it on a single crystal of tetracene[176] or on a polycrystalline layer of pentacene.[177] However, using other semiconductor molecules as templates is not appropriate because, as mentioned, the first monolayers at the organic semiconductor/dielectric interface are responsible for the device performance. Miao and colleagues[178] have recently published the use of a 3 nm thick layer of 6,13-pentacenequinone (PQ), an easily crystallized insulating molecule, on octadecylphosphonic acid-treated SiO_2 as a template to induce the crystallization of rubrene in vacuum-deposited thin films. The AFM images in Figure 33 clearly show that the rubrene films only form large crystal-shaped domains in these conditions. The OFET mobility of such films was up to 0.35 $cm^2/(V\ s)$.

dx.doi.org/10.1021/cr100142w |*Chem. Rev.* 2011, 111, 4833–4856

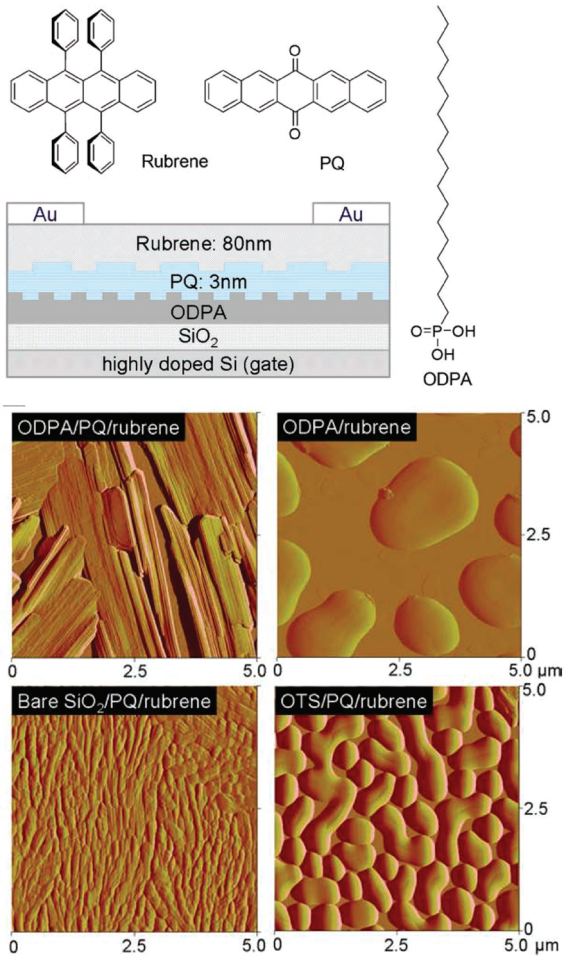

Figure 33. (Top) Device architecture of the thin-film transistors of rubrene with a template layer of PQ. (Bottom) AFM amplitude images of rubrene thin films on varied surfaces. The thickness of the rubrene films is 80 nm. Reprinted with permission from ref 178. Copyright 2010 Wiley-VCH Verlag GmbH & Co.

5.2. Organic Semiconductor/Metal Interface

Similarly, the structure at the metal/organic semiconductor interface has also been investigated, as in the case of α,ω-diperfluorohexylquaterthiophene (DFH-4T). Here, dramatic morphology and molecular orientation changes were observed when going from a monolayer to a multilayer film. Furthermore, it was observed that DFH-4T growth on Au and SiO_2 in a bottom-contact configuration creates additional film discontinuities and potential electron traps. All this was attributed to be the cause of why the mobility achieved in bottom-contact OFETs was 3 orders of magnitude lower than in top-contact OFETs.[179]

It is widely known that pentacene, the benchmark in the field of OFETs, has given rise to elevated mobilities. Nonetheless, such high performances have only been successfully achieved in devices with top-contact geometries by evaporating the source and drain electrodes on pentacene films through a shadow mask. In a bottom-contact geometry a crucial problem arises since on the top of the metal electrodes pentacene growth is disrupted, preferring to lie flat on the metal surface, which is detrimental for the OFET performance. However, it has been demonstrated that by modifying the metal characteristics with a SAM, the thin-film morphology can be tailored.[180] Good field-effect characteristics were reached when the orientation of pentacene on and next to the modified metal electrodes was identical to the orientation of the pentacene on the SiO_2 dielectric. Nevertheless, it should be taken into account that it has also been observed that the charge carrier mobility exhibits large fluctuations with the length of the alkanethiol SAMs and that an odd−even effect ascribed to the anisotropic coupling between the alkanethiol terminal σ bond and the HOMO level of ordered pentacene molecules takes place.[181]

6. SUMMARY

In the near future organic field-effect transistors are bound to make a huge impact in the microelectronics industry in applications where low-cost and large area coverage are required. However, contrary to their inorganic counterparts where the atoms are held together by strong covalent bonds, the interactions between molecules in organic semiconductors are much weaker. Such intermolecular interactions are responsible for the formation of a conduction path, and therefore, the mobility in organic materials is highly dependent on the molecular ordering. Indeed, small structural modifications, which can be caused by tiny molecular changes or even by varying the experimental fabrication conditions, can be the key for achieving a high OFET performance. Currently, great efforts are being devoted to the understanding of the transport mechanisms and the structure/performance correlation, where, undoubtedly, due to their high molecular order single-crystal devices represent ideal systems and also permit a direct comparison between theory and experiment. To progress in the field of organic electronics, it is thus imperative to gain a better insight into the influence of the intermolecular interactions on the solid-state structure and the transport properties so it will be feasible to design materials for specific applications.

AUTHOR INFORMATION

Corresponding Author

*Phone: +34 935801853. Fax: +34 935805729. E-mail: mmas@icmab.es (M.M.-T.); cun@icmab.es (C.R.).

BIOGRAPHIES

Marta Mas-Torrent received her Ph.D. in 2002 working at the Institut de Ciència de Materials, Consejo Superior de Investigacions Científicas (ICMAB-CSIC) in Barcelona, Spain, and at The Royal Institution of Great Britain in London, U.K. Afterward, she carried out postdoctoral research at the Kavli Institute of

Nanoscience, Delft, The Netherlands. In November 2004 she came back to ICMAB with a Ramón y Cajal fellowship, and in June 2007 she obtained a tenured research position at ICMAB-CSIC. Her scientific interests include molecular electronics, organic field-effect transistors, multifunctional molecular materials, molecular switches and memory devices, self-assembly, and surface molecular organizations.

Dr. Concepció Rovira received her Ph.D. in chemistry from the University of Barcelona. She trained as a postdoctoral fellow at CSIC in Barcelona and at Johns Hopkins University with Prof. D. O. Cowan. In 1987 she joined CID-CSIC with a tenured research position and became Full Professor at ICMAB-CSIC in 2004. Her research interests focus on multifunctional molecular materials and molecular nanoscience and in particular on the fields of organic conductors, crystal engineering, supramolecular and surface self-assembly, electron transfer processes, and molecular magnetism.

ACKNOWLEDGMENT

We thank R. Pfattner, Dr. N. Crivillers, and Prof. J. Veciana for their help. We also thank the European Union Large Project One-P (Grant FP7-NMP-2007-212311), the Networking Research Center on Bioengineering, Biomaterials and Nanomedicine (CIBER-BBN), the Direccion General de Investigación (DGI) (Spain) for Projects CTQ2006-06333/BQU and CTQ2010-195011/BQU, and Generalitat de Catalunya (Grant 2009SGR516).

REFERENCES

(1) (a) Sirringhaus, H. *Adv. Mater.* **2005**, *17*, 2411. (b) Horowitz, G. *J. Mater. Res.* **2004**, *19*, 1946.

(2) (a) Mas-Torrent, M.; Rovira, C. *Chem. Soc. Rev.* **2008**, *37*, 827. (b) Dimitrakopoulos, C. D.; Malenfant, P. R. L. *Adv. Mater.* **2002**, *14*, 99. (c) Sun, Y.; Liu, Y.; Zhu, D. *J. Mater. Chem.* **2005**, *15*, 53. (d) Katz, H. E. *Chem. Mater.* **2004**, *16*, 4748. (e) Singh, Th. B.; Sariciftci, N. S. *Annu. Rev. Mater. Res.* **2006**, *36*, 199.

(3) (a) Braun, S.; Salaneck, W. R.; Fahlman, M. *Adv. Mater.* **2009**, *21*, 1450. (b) Shibata, K.; Ishikawa, K.; Takezoe, H.; Wada, H.; Mori, T. *Appl. Phys. Lett.* **2008**, *92*, 023305.

(4) Yoon, M.-Y.; Facchetti, A.; Marks, T. J. *J. Am. Chem. Soc.* **2006**, *128*, 12851.

(5) Park, Y. D.; Lim, J. A.; Lee, H. S.; Cho, K. *Materials Today* **2007**, *10*, 46.

(6) DiBenedetto, S. A.; Facchetti, A.; Ratner, M. A.; Marks, T. *Adv. Mater.* **2009**, *21*, 1407.

(7) Marcus, R. A. *Rev. Mod. Phys.* **1993**, *65*, 599. (b) Gruhn, N. E.; da Silva Filho, D. A.; Bill, T. G.; Malagoli, M.; Coropceanu, V.; Kahn, A.; Brédas, J.-L. *J. Am. Chem. Soc.* **2002**, *124*, 7918.

(8) Coropceanu, V.; Cornil, J.; Da Silva Filho, D. A.; Olivier, Y.; Silbey, R.; Brédas, J. L. *Chem. Rev.* **2007**, *107*, 926.

(9) (a) Valeev, E. F.; Coropceanu, V.; Silva, D. A. d.; Salman, S.; Brédas, J.-L. *J. Am. Chem. Soc.* **2006**, *128*, 9882–9886. (b) Senthilkumar, K.; Grozema, F. C.; Bickelhaupt, F. M.; Siebbeles, L. D. A. *J. Chem. Phys.* **2003**, *119*, 9809–9817.

(10) Coropceanu, V.; Malagoli, M.; da Silva Filho, D. A.; Gruhn, N. E.; Bill, T. G.; Brédas, J. L. *Phys. Rev. Lett.* **2002**, *89*, 275503.

(11) Marcus, R. A. *J. Chem. Phys.* **1965**, *43*, 679–701.

(12) Lemaur, V.; da Silva Filho, D. A.; Coropceanu, V.; Lehmann, M.; Geerts, Y.; Piris, J.; Debije, M. G.; van de Craats, A. M.; Senthilkumar, K.; Siebbeles, L. D. A.; Warman, J. M.; Brédas, J. L.; Cornil, J. *J. Am. Chem. Soc.* **2004**, *126*, 3271–3279.

(13) Bromley, S. T.; Mas-Torrent, M.; Hadley, P.; Rovira, C. *J. Am. Chem. Soc.* **2004**, *126*, 6544.

(14) Bromley, S. T.; Illas, F.; Mas-Torrent, M. *Phys. Chem. Chem. Phys.* **2008**, *10*, 121.

(15) Tsao, H. N.; Mullen, K. *Chem. Soc. Rev.* **2010**, *39*, 2372.

(16) McCullough, R. D. *Adv. Mater.* **1998**, *10*, 93.

(17) Sirringhaus, H.; Brown, P. J.; Friend, R. H.; Nielsen, M. M.; Bechgaard, K.; Langeveld-Voss, B. M. W.; Spiering, A. J. H.; Janssen, R. A. J.; Meijer, E. W.; Herwig, P.; de Leeuw, D. M. *Nature* **1999**, *401*, 685.

(18) Allard, S.; Forster, M.; Souharce, B.; Thiem, H.; Scherf, U. *Angew. Chem., Int. Ed.* **2008**, *47*, 4070.

(19) Wang, G.; Swensen, J.; Moses, D.; Heeger, A. J. *J. Appl. Phys.* **2003**, *93*, 6137.

(20) Mena-Osteritz, E.; Meyer, A.; Langeveld-Voss, B. M. W.; Janssen, R. A. J.; Meijer, E. W.; Bäuerle, P. *Angew. Chem., Int. Ed.* **2000**, *39*, 2680.

(21) Bao, Z.; Dodabalapur, A.; Lovinger, A. J. *Appl. Phys. Lett.* **1996**, *69*, 4108.

(22) Ihn, K. J.; Moulton, J.; Smith, P. *J. Polym. Sci., Part B: Polym. Phys.* **1993**, *31*, 735.

(23) (a) Merlo, J. A.; Frisbie, C. D. *J. Phys. Chem. B* **2004**, *108*, 19169. (b) Merlo, J. A.; Frisbie, C. D. *J. Polym. Sci., Part B: Polym. Phys.* **2003**, *41*, 2674.

(24) Leclère, Ph.; Hennebicq, E.; Calderone, A.; Brocorens, P.; Grimsdale, A. C.; Müllen, K.; Brédas, J. L.; Lazzaroni, R. *Prog. Polym. Sci.* **2003**, *28*, 55.

(25) (a) Kline, J. R.; McGehee, M. D.; Kadnikova, E. N.; Liu, J.; Fréchet, J. M. J. *Adv. Mater.* **2003**, *15*, 1519. (b) Zen, A.; Pflaum, J.; Hirschmann, S.; Zhuang, W.; Jaiser, F.; Asawapirom, U.; Rabe, J. P.; Scherf, U.; Neher, D. *Adv. Funct. Mater.* **2004**, *14*, 757.

(26) Nagamatsu, S.; Takashima, W.; Kaneto, K.; Yoshida, Y.; Tanigaki, N.; Yase, K.; Omote, K. *Macromolecules* **2003**, *36*, 5252.

(27) (a) Derue, G.; Copée, S.; Gabriele, S.; Surin, M.; Geskin, V.; Monteverde, F.; Leclère, Ph.; Lazzaroni, R.; Damman, P. *J. Am. Chem. Soc.* **2005**, *127*, 8018. (b) Derue, G.; Serban, D. A.; Leclère, Ph.; Melinte, S.; Damman, P.; Lazzaroni, R. *Org. Electron.* **2008**, *9*, 821.

(28) Jimison, L. H.; Toney, M. F.; McCulloch, I.; Heeney, M.; Salleo, M. *Adv. Mater.* **2009**, *21*, 1568.

(29) Fong, H. H.; Pozdin, V. A.; Amassian, A.; Malliaras, G. G.; Smilgies, D. M.; He, M.; Gasper, S.; Zhang, F.; Sorensen, M. *J. Am. Chem. Soc.* **2008**, *130*, 13202.

(30) Tsao, H. N.; Cho, D.; Andreasen, J. W.; Rouhanipour, A.; Breiby, D. W.; Pisula, W.; Mullen, K. *Adv. Mater.* **2009**, *21*, 209.

(31) McCulloch, I.; Heeney, M.; Bailey, C.; Genevicius, K.; Macdonald, I.; Schkunov, M.; Sparrowe, D.; Tierney, S.; Wagner, R.; Zhang, W.; Chabinyc, M. L.; Kline, R. J.; McGehee, M. D.; Toney, M. F. *Nat. Mater.* **2006**, *5*, 328.

(32) (a) Veres, J.; Ogier, S.; Lloyd, G. *Chem. Mater.* **2004**, *16*, 4543. (b) Veres, J.; Ogier, S. D.; Leeming, S. W.; Cupertino, D. C.; Khaffaf, S. M. *Adv. Funct. Mater.* **2003**, *13*, 199.

(33) Zhang, M.; Tsao, H. N.; Pisula, W.; Yang, C.; Mishra, A. K.; Müllen, K. J. *Am. Chem. Soc.* **2007**, *129*, 3472.

(34) Liu, J.; Zhang, R.; Sauvé, G.; Kowalewski, T.; McCulloch, R. D. *J. Am. Chem. Soc.* **2008**, *130*, 13167.

(35) Yan, H.; Chen, Z.; Newman, C.; Quinn, J. R.; Dötz, F.; Kastler, M.; Facchetti, A. *Nature* **2009**, *457*, 679.
(36) Tessler, N.; Preezant, Y.; Rappaport, N.; Roichman, Y. *Adv. Mater.* **2009**, *21*, 2741.
(37) Dimitrakopoulos, C. D.; Mascaro, D. J. *IBM J. Res. Dev.* **2001**, *45*, 11.
(38) Xiao, K.; Liu, Y.; Yu, G.; Zhu, D. *Appl. Phys. A: Mater. Sci. Process.* **2003**, *77*, 367.
(39) Rivnay, J.; Jimison, L. H.; Northrup, J. E.; Toney, M. F.; Noriega, R.; Lu, S.; Marks, T. J.; Facchetti, A.; Salleo, A. *Nat. Mater.* **2009**, *8*, 952.
(40) Ling, M. M.; Bao, Z. *Chem. Mater.* **2004**, *16*, 4824.
(41) Dimitrakopoulos, C. D.; Brown, A. R.; Pomp, A. J. *J. Appl. Phys.* **1996**, *80*, 2501.
(42) Xue, J.; Forrest, S. R. *Appl. Phys. Lett.* **2001**, *79*, 3714.
(43) Youn, J.; Chen, M.-C.; Liang, Y.-j.; Huang, H.; Ponce Ortiz, R.; Kim, C.; Stern, C.; Hu, T.-S.; Chen, L.-H.; Yan, J.-Y.; Facchetti, A.; Marks, T. J. *Chem. Mater.* **2010**, *22*, 5031.
(44) Lim, J. A.; Lee, H. S.; Lee, W. W.; Cho, K. *Adv. Funct. Mater.* **2009**, *19*, 1515.
(45) (a) Miskiewicz, P.; Mas-Torrent, M.; Jung, J.; Kotarba, S.; Glowacki, I.; Gomar-Nadal, E.; Amabilino, D. B.; Rovira, C.; Veciana, J.; Krause, B.; Carbone, D.; Ulanski, J. *Chem. Mater.* **2006**, *18*, 4724. (b) Mas-Torrent, M.; Masirek, S.; Hadley, P.; Crivillers, N.; Oxtoby, N. S.; Reuter, P.; Veciana, J.; Rovira, C.; Tracz, A. *Org. Electron.* **2008**, *9*, 143. (c) Pisula, W.; Menon, A.; Stepputat, M.; Lieberwirth, I.; Kolb, U.; Tracz, A.; Sirringhaus, H.; Pakula, T.; Müllen, K. *Adv. Mater.* **2005**, *17*, 684. (d) Duffy, C. M.; Andreasen, J. W.; Breiby, D. W.; Nielsen, M. M.; Ando, M.; Minakata, T.; Sirringhaus, H. *Chem. Mater.* **2008**, *20*, 7252.
(46) Sele, C. W.; Kjellander, B. K. C.; Niesen, B.; Thornton, M. J.; van der Putten, J. B. P. H.; Myny, K.; Wondergem, H. J.; Moser, A.; Resel, R.; van Breemen, A. J. J. M.; van Aerle, N.; Heremans, P.; Anthony, J. E.; Gelinck, G. H. *Adv. Mater.* **2009**, *21*, 4926.
(47) Becerril, H. A.; Roberts, M. E.; Liu, Z.; Locklin, J.; Bao, Z. *Adv. Mater.* **2008**, *20*, 2588.
(48) Cavallini, M.; Stoliar, P.; Moulin, J. F.; Surin, M.; Leclère, P.; Lazzaroni, R.; Breiby, D. W.; Andreasen, J. W.; Nielsen, M. M.; Sonar, P.; Grimsdale, A. C.; Mullen, K.; Biscarini, F. *Nano Lett.* **2005**, *5*, 2422.
(49) Rancatore, B. J.; Mauldin, C. E.; Tung, S.-H.; Wang, C.; Hexemer, A.; Strzalka, J.; Fréchet, J. M. J.; Xu, T. *ACS Nano* **2010**, *4*, 2721.
(50) Lee, W. H.; Lim, J. A.; Kim, D. H.; Cho, J. H.; Jang, Y.; Kim, Y. H.; Ham, J. I.; Cho, K. *Adv. Funct. Mater.* **2008**, *18*, 560.
(51) Dickey, K. C.; Anthony, J. E. *Adv. Mater.* **2006**, *18*, 1721.
(52) Di, C.; Lu, K.; Zhang, L.; Liu, Y.; Guo, Y.; Sun, X.; Wen, Y.; Yu, G.; Zhu, D. *Adv. Mater.* **2010**, *22*, 1273.
(53) Stingelin-Stutzmann, N.; Smits, E.; Wondergem, H.; Tanase, C.; Blom, P.; Smith, P.; De Leeuw, D. *Nat. Mater.* **2005**, *4*, 601.
(54) Würtner, F.; Schmidt, R. *ChemPhysChem.* **2006**, *7*, 793.
(55) Payne, M. M.; Parkin, S. R.; Anthony, J. E.; Kuo, C.-C.; Jackson, T. N. *J. Am. Chem. Soc.* **2005**, *127*, 4986.
(56) Ando, S.; Murakami, R.; Nishida, J.; Tada, H.; Inoue, Y.; Tokito, S.; Yamashita, Y. *J. Am. Chem. Soc.* **2005**, *127*, 14996.
(57) (a) Moon, H.; Zeis, R.; Borkent, E.-J.; Besnard, C.; Lovinger, A. J.; Siegrist, T.; Kloc, C.; Bao, Z. *J. Am. Chem. Soc.* **2004**, *126*, 15322. (b) Chi, X.; Li, D.; Zhang, H.; Chen, Y.; Garcia, V.; Garcia, C.; Siegrist, T. *Org. Electron.* **2008**, *9*, 234. (c) Reese, C.; Roberts, M. E.; Parkin, S. R.; Bao, Z. *Adv. Mater.* **2009**, *21*, 3678.
(58) (a) Bredas, J.-L.; Beljonne, D.; Coropceanu, V.; Cornil, J. *Chem. Rev.* **2004**, *147*, 4971.
(59) Minari, T.; Seto, M.; Nemoto, T.; Isoda, S.; Tsukagoshi, K.; Aoyagi, Y. *Appl. Phys. Lett.* **2007**, *91*, 123501.
(60) Curtis, M. D.; Cao, J.; Kampf, J. W. *J. Am. Chem. Soc.* **2004**, *126*, 4318.
(61) Hutchison, G. R.; Ratner, M. A.; Marks, T. J. *J. Am. Chem. Soc.* **2005**, *127*, 16866.
(62) (a) Yamamoto, T.; Takimiya, K. *Bull. Chem. Soc. Jpn.* **2010**, *83*, 120. (b) Yamamoto, T.; Takimiya, K. *J. Am. Chem. Soc.* **2007**, *129*, 2224.
(63) (a) Brédas, J. L.; Calbert, J. P.; da Silva Filho, D. A.; Cornil, J. *Proc. Natl. Acad. Sci. U.S.A.* **2002**, *99*, 5804. (b) Kwon, O.; Coropceanu, V.; Gruhn, N. E.; Durivage, J. C.; Laquindanum, J. G.; Katz, H. E.; Cornil, J.; Brédas, J. L. *J. Chem. Phys.* **2004**, *120*, 8186.
(64) Li, R.; Hu, W.; Liu, Y.; Zhu, D. *Acc. Chem. Res.* **2010**, *43*, 529.
(65) Jiang, L.; Fu, Y. Y.; Li, H. X.; Hu, W. P. *J. Am. Chem. Soc.* **2008**, *130*, 3937.
(66) Subramanian, S.; Park, S. Y.; Parkin, S. R.; Podzorov, V.; Jackson, T. N.; Anthony, J. E. *J. Am. Chem. Soc.* **2008**, *130*, 2706.
(67) Briseno, A. L.; Mannsfeld, S. C. B.; Xiong, X.; Lu, Y.; Jenekhe, S. A.; Bao, Z.; Xia, Y. *Nano Lett.* **2007**, *7*, 668.
(68) Sun, Y. M.; Tan, L.; Jiang, S. D.; Qian, H. L.; Wang, Z. H.; Yan, D. W.; Di, C. G.; Wang, Y.; Wu, W. P.; Yu, G.; Yan, S. K.; Wang, C. R.; Hu, W. P.; Liu, Y. Q.; Zhu, D. B. *J. Am. Chem. Soc.* **2007**, *129*, 1882.
(69) Kunugi, Y.; Takimiya, K.; Yamane, K.; Yamashita, K.; Aso, Y.; Otsubo, T. *Chem. Mater.* **2003**, *15*, 6.
(70) (a) Takimiya, K.; Kunugi, Y.; Konda, Y.; Ebata, H.; Toyoshima, Y.; Otsubo, T. *J. Am. Chem. Soc.* **2006**, *128*, 3044. (b) Yamamoto, T.; Takimiya, K. *J. Am. Chem. Soc.* **2007**, *129*, 2224.
(71) Takimiya, K.; Kunugi, Y.; Konda, Y.; Niihara, N.; Otsubo, T. *J. Am. Chem. Soc.* **2004**, *126*, 5084.
(72) Jiang, L.; Dong, H.; Hu, W. *J. Mater. Chem.* **2010**, *20*, 4994.
(73) (a) Reese, C.; Bao, Z. *J. Mater. Chem.* **2006**, *16*, 329. (b) Reese, C.; Bao, Z. *Mater. Today* **2007**, *10*, 20.
(74) De Boer, R. W. I.; Gershenson, M. E.; Morpurgo, A. F.; Podzorov, V. *Phys. Status Solidi A* **2004**, *201*, 1302.
(75) Kloc, C.; Simpkins, P. G.; Siegrist, T.; Laudise, R. A. *J. Cryst. Growth* **1997**, *182*, 416.
(76) De Boer, R. W. I.; Klapwijk, T. M.; Morpurgo, A. F. *Appl. Phys. Lett.* **2003**, *83*, 4345.
(77) Molinari, A. S.; Alves, H.; Chen, Z.; Fachetti, A.; Morpurgo, A. F. *J. Am. Chem. Soc.* **2009**, *131*, 2462.
(78) Sundar, V. C.; Zaumseil, J.; Podzorov, V.; Menard, E.; Willett, R. L.; Someya, T.; Gershenson, M. E.; Rogers, J. A. *Science* **2004**, *303*, 1644.
(79) Podzorov, V.; Menard, E.; Borissov, A.; Kiryukhin, V.; Rogers, J. A.; Gerhenson, M. E. *Phys. Rev. Lett.* **2004**, *93*, 086602.
(80) Mas-Torrent, M.; Rovira, C. *J. Mater. Chem.* **2006**, *16*, 433.
(81) (a) Mas-Torrent, M.; Durkut, M.; Hadley, P.; Ribas, X.; Rovira, C. *J. Am. Chem. Soc.* **2004**, *126*, 984. (b) Mas-Torrent, M.; Hadley, P.; Bromley, S. T.; Ribas, X.; Tarrés, J.; Mas, M.; Molins, E.; Veciana, J.; Rovira, C. *J. Am. Chem. Soc.* **2004**, *126*, 8546. (c) Leufgen, M.; Rost, O.; Gould, C.; Schmidt, G.; Geurts, J.; Molenkamp, L. W.; Oxtoby, N. S.; Mas-Torrent, M.; Crivillers, N.; Veciana, J.; Rovira, C. *Org. Electron.* **2008**, *9*, 1101. (d) Mas-Torrent, M.; Hadley, P.; Bromley, S. T.; Crivillers, N.; Veciana, J.; Rovira, C. *Appl. Phys. Lett.* **2005**, *86*, 012110.
(82) Kim, D. H.; Lee, D. Y.; Lee, W. S.; Lee, W. H.; Kim, Y. H.; Han, J. I.; Cho, K. *Adv. Mater.* **2007**, *19*, 678.
(83) Da Silva Filho, D. A.; Kim, E.-G.; Brédas, J.-L. *Adv. Mater.* **2005**, *17*, 1072.
(84) Reese, C.; Bao, Z. *Adv. Mater.* **2007**, *19*, 4535.
(85) Lee, J. Y; Roth, S.; Park, Y. W. *Appl. Phys. Lett.* **2006**, *88*, 252106.
(86) Yin, S.; Lv, Y. *Org. Electron.* **2008**, *9*, 852.
(87) Xia, Y.; Kalihari, V.; Frisbie, D.; Oh, N. K.; Rogers, J. A. *Appl. Phys. Lett.* **2007**, *90*, 162106.
(88) Zeis, R.; Besnard, C.; Siegrist, T.; Scholockermann, C.; Chi, X.; Kloc, C. *Chem. Mater.* **2006**, *18*, 244.
(89) Fraboni, B.; Femoni, C.; Mencarelli, I.; Setti, L.; Di Pietro, R.; Cavallini, A.; Fraleoni-Morgera, A. *Adv. Mater.* **2009**, *21*, 1835.
(90) Wang, Y.; Kumashiro, R.; Li, Z.; Nouchi, R.; Tanigaki, K. *Appl. Phys. Lett.* **2009**, *95*, 103306.
(91) Mannsfeld, S. C. B.; Locklin, J.; Reese, C.; Roberts, M. E.; Lovinger, A. J.; Bao, Z. *Adv. Funct. Mater.* **2007**, *17*, 1617.

(92) Jiang, L.; Gao, J. H.; Wang, J.; Li, H. X.; Wang, Z. H.; Hu, W. P.; Jiang, L. *Adv. Mater.* **2008**, *20*, 2735.
(93) Jiang, L.; Hu, W.; Wei, Z.; Xu, W.; Meng, H. *Adv. Mater.* **2009**, *21*, 3649.
(94) Li, R.; Jiang, L.; Meng, Q.; Gao, J.; Li, H.; Tang, Q.; He, M.; Hu, W.; Liu, Y.; Zhu, D. *Adv. Mater.* **2009**, *21*, 4492.
(95) Uno, M.; Tominari, Y.; Doi, I.; Miyazaki, E.; Takimiya, K.; Takeya, J. *Appl. Phys. Lett.* **2009**, *94*, 223308.
(96) (a) Tessler, N.; Roichman, Y. *Appl. Phys. Lett.* **2001**, *79*, 2987. (b) Richards, T. J.; Sirringhaus, H. *J. Appl. Phys.* **2007**, *102*, 094510.
(97) Braga, D.; Horowitz, G *Adv. Mater.* **2009**, *21*, 1473.
(98) Takahashi, Y.; Hasegawa, T.; Horiuchi, S.; Kumai, R.; Tokura, Y; Saito, G. *Chem. Mater.* **2007**, *19*, 6382.
(99) Briseno, A. L.; Mannsfeld, S. C. B.; Ling, M. M.; Liu, S. H.; Tseng, R. J.; Reese, C.; Roberts, M. E.; Yang, Y.; Wudl, F.; Bao, Z. N. *Nature* **2006**, *444*, 913.
(100) Tang, Q. X.; Li, H. X.; Song, Y. B.; Xu, W.; Hu, W. P.; Jiang, L.; Liu, Y. Q.; Wang, X. K.; Zhu, D. B. *Adv. Mater.* **2006**, *18*, 3010.
(101) Tang, Q. X.; Li, H. X.; Liu, Y. L.; Hu, W. P. *J. Am. Chem. Soc.* **2006**, *128*, 14634.
(102) Briseno, A. L.; Aizenberg, J.; Han, Y. J.; Penkala, R. A.; Moon, H.; Lovinger, A. J.; Kloc, C.; Bao, Z. A. *J. Am. Chem. Soc.* **2005**, *127*, 12164.
(103) Liu, S. H.; Wang, W. C. M.; Mannsfeld, S. C. B.; Locklin, J.; Erk, P.; Gomez, M.; Richter, F.; Bao, Z. N. *Langmuir* **2007**, *23*, 7428.
(104) Liu, S.; Wang, W. M.; Briseno, A. L.; Mannsfeld, S. C. B.; Bao, Z. *Adv. Mater.* **2009**, *21*, 1217.
(105) Noda, B.; Wada, H.; Shibata, K.; Yoshino, T.; Katsuhara, M.; Aoyagi, I.; Mori, T.; Taguchi, T.; Kambayashi, T.; Ishikawa, K.; Takezoe, H. *Nanotechnology* **2007**, *18*, 424009.
(106) Berstein, J. *Polymorphism in Molecular Crystals*; Clarendon Press: Oxford, U.K., 2002.
(107) Threlfall, T. L. *Analyst* **1995**, *120*, 2435.
(108) Pfattner, R.; Mas-Torrent, M.; Bilotti, I.; Brillante, A.; Milita, S.; Liscio, F.; Biscarini, F.; Marszalek, T.; Ulanski, J.; Nosal, A.; Gazicki-Lipman, M.; Leufgen, M.; Schmidt, G.; Molenkamp, L. W.; Laukhin, V.; Veciana, J.; Rovira, C. *Adv. Mater.* **2010**, *22*, 4198.
(109) Jurchescu, O. D.; Mourey, D. A.; Subramanian, S.; Parkin, S. R.; Vogel, B. M.; Anthony, J. E.; Jackson, T. N.; Gundlach, D. J. *Phys. Rev. B* **2009**, *80*, 085201.
(110) Jiang, H.; Yang, X.; Cui, Z.; Liu, Y.; Li, H.; Hu, W.; Liu, Y.; Zhu, D. *Appl. Phys. Lett.* **2007**, *91*, 123505.
(111) Matsukawa, T.; Yoshimura, M.; Sasai, K.; Uchiyama, M.; Yamagishi, M.; Tominari, Y.; Takahashi, Y.; Takeya, J.; Kitaoka, Y.; Mori, Y.; Sasaki, T. *J. Cryst. Growth* **2010**, *312*, 310.
(112) Campbell, R. B.; Roberston, J. M.; Trotter, J. *Acta Crystallogr.* **1961**, *14*, 705.
(113) (a) Holmes, D.; Kumaraswamy, S.; Matzger, A. J.; Vollhardt, K. P. C. *Chem.—Eur. J.* **1999**, *5*, 3399. (b) Siergrist, T.; Kloc, C.; Schön, H. J.; Batlogg, B.; Haddon, R. C.; Berg, S.; Thomas, G. A. *Angew. Chem.* **2001**, *40*, 1732. (c) Mattheus, C. C.; Dros, A. B.; Baas, J.; Meetsma, A.; de Boer, J. L.; Palstra, T. T. M. *Acta Crystallogr., Sect. C* **2001**, *57*, 939.
(114) (a) Brillante, A.; Della Valle, R. G.; Farina, L.; Girlando, A.; Masino, M.; Venuti, E. *Chem. Phys. Lett.* **2002**, *357*, 32. (b) Brillante, A.; Bilotti, I.; Della Valle, R. G.; Venuti, E.; Masino, M.; Girlando, A. *Adv. Mater.* **2005**, *17*, 2549.
(115) Farina, L.; Brillante, A.; Della Valle, R. G.; Venuti, E.; Amboage, M.; Syassen, K. *Chem. Phys. Lett.* **2003**, *375*, 490.
(116) Brillante, A.; Bilotti, I.; Della Valle, R. G.; Venuti, E.; Masino, M.; Girlando, A. *CrystEngComm* **2008**, *10*, 937.
(117) Della Valle, R. G.; Venuti, E.; Brillante, A.; Girlando, A. *J. Chem. Phys.* **2003**, *118*, 807.
(118) (a) Siegrist, T.; Besnard, C.; Haas, S.; Schiltz, M.; Pattison, P.; Chernyshow, D.; Batlogg, B.; Kloc, C. *Adv. Mater.* **2007**, *19*, 2079. (b) Mattheus, C. C.; Dros, A. B.; Baas, J.; Oostergetel, G. T.; Meetsma, A.; de Boer, J. L.; Palstra, T. T. M. *Synth. Met.* **2003**, *138*, 475.
(119) Alternalively, Herbstein designates pentacene LT as EI and pentacene HT as EII: Herbstein, F. A. *Acta Crystallogr., Sect. B* **2006**, *62*, 341.
(120) Mattheus, C. C.; de Wijs, G. A.; de Groot, R. A.; Palstra, T. T. M. *J. Am. Chem. Soc.* **2003**, *125*, 6323.
(121) (a) Bouchoms, I. P. M.; Schoonveld, W. A.; Vrijmoeth, J.; Klapwiijk, T. M. *Synth. Met.* **1999**, *104*, 175. (b) Ruiz, R.; Choudhary, D.; Nickel, B.; Toccoli, T.; Chang, K.-S.; Mayer, A. C.; Claney, P.; Blakely, J. M.; Headrick, R. L.; Iannotta, S.; Malliaras, G. G. *Chem. Mater.* **2004**, *16*, 4497. (c) Guo, D.; Ikeda, S.; Saiki, K. *Thin Solid Films* **2006**, *515*, 814. (d) Steudel, S.; De Vusser, S.; De Jonge, S.; Janssen, D.; Verlaak, S.; Genoe, J.; Heremans, P. *Appl. Phys. Lett.* **2004**, *85*, 4400. (e) Kim, C.; Facchetti, A.; Marks, T. J. *Science* **2007**, *318*, 76.
(122) Kakudate, T.; Yoshimoto, N.; Saito, Y. *Appl. Phys. Lett.* **2007**, *90*, 081903.
(123) Kim, D. H.; Lee, H. S.; Yang, H.; Yang, L.; Cho, K. *Adv. Funct. Mater.* **2008**, *18*, 1363.
(124) Campbell, R. B.; Roberston, J. M.; Trotter, J. *Acta Crystallogr.* **1962**, *15*, 289.
(125) Jankowiak, R.; Kalinowski, J.; Konys, M.; Buchert, J. *Chem. Phys. Lett.* **1979**, *65*, 549.
(126) Venuti, E.; Della Valle, R. G.; Farina, L.; Brillante, A.; Masino, M.; Girlando, A. *Phys. Rev. B* **2004**, *70*, 104106.
(127) Sonderman, U.; Kutoglu, A.; Bässler, H. *J. Phys. Chem.* **1985**, *89*, 1735.
(128) Kalinowski, J.; Jankowiak, R. *Chem. Phys. Lett.* **1978**, *53*, 56.
(129) Rang, Z.; Haraldsson, A.; Kim, D. M.; Ruden, P. P.; Natham, M. I.; Chesterfield, J.; Frisbie, C. D. *Appl. Phys. Lett.* **2001**, *79*, 2731.
(130) Yuan, Q.; Mannsfeld, S. C. B.; Tang, M.; Toney, M. F.; Luning, J.; Bao, Z. *J. Am. Chem. Soc.* **2008**, *130*, 3502.
(131) Valiyev, F.; Hu, W.-S.; Chen, H.-Y.; Kuo, M.-Y.; Chao, Y.; Tao, Y.-T. *Chem. Mater.* **2007**, *19*, 3018.
(132) Tang, M. I.; Okamoto, T.; Bao, Z. *J. Am. Chem. Soc.* **2006**, *128*, 16002.
(133) (a) Bulgarovskaya, I.; Vozzhennikov, V.; Aleksandrov, S.; Belsky, V. *Latv. PSR Zinat. Akad. Vestis, Kim. Ser.* **1983**, *4*, 53. (b) Jurchescu, O. D.; Meetsma, A.; Palstra, T. T. M. *Acta Crystallogr., Sect. B* **2006**, *62*, 330. (c) Taylor, W. H. *Z. Kristallogr.* **1936**, *93*, 151. (c) Akopjan, R. L.; Kitaigordskii, A. I.; Struchkov, Y. T. *Zh. Strukt. Khim.* **1962**, *3*, 602.
(134) Huang, L.; Liao, Q.; Shi, Q.; Fu, H.; Ma, J.; Yao, J. *J. Mater. Chem.* **2010**, *20*, 159.
(135) Heinrich, M. A.; Pflaum, J.; Tripathi, A. K.; Frey, W.; Steigerwald, M. L.; Siegrist, T. *J. Phys. Chem. C* **2007**, *111*, 18878.
(136) Dürr, A. C.; Schreiber, F.; Münch, M.; Karl, N.; Krause, B.; Kruppa, V.; Dosch, H. *Appl. Phys. Lett.* **2002**, *81*, 2276.
(137) Tripathi, A. K.; Pflaum, J. *Appl. Phys. Lett.* **2006**, *89*, 082103.
(138) (a) Visser, G. J.; Heeres, G. J.; Wolters, J.; Vos, A. *Acta Crystallogr., Sect. B* **1968**, *24*, 467. (b) Chaloner, P. A.; Gunatunga, S. R.; Hitchcock, P. B. *Acta Crystallogr., Sect. C* **1994**, *50*, 1941. (c) Pelletier, M.; Brisse, F. *Acta Crystallogr., Sect. C* **1994**, *50*, 1942.
(139) Porzio, W.; Destri, S.; Mascherpa, M.; Rossini, S.; Bruckner, S. *Synth. Met.* **1993**, *55*, 408.
(140) Siegrist, T.; Kloc, C.; Laudise, R. A.; Katz, H. E.; Haddon, R. C. *Adv. Mater.* **1998**, *10*, 379.
(141) Antolini, L.; Horowitz, G.; Kouki, F.; Garnier, F. *Adv. Mater.* **1998**, *10*, 382.
(142) Ranzieri, P.; Girlando, A.; Tavazzi, S.; Campione, M.; Raimondo, L.; Bilotti, I.; Brillante, A.; Della Valle, R- G.; Venuti, E. *ChemPhysChem* **2009**, *10*, 657.
(143) Hermet, P.; Hizard, N.; Rahmani, A.; Ghosez, Ph. *J. Phys. Chem. A* **2005**, *109*, 4202.
(144) Hermet, P.; Bantignies, J. L.; Sauvajol, J. L.; Johnson, M. R. *Synth. Met.* **2006**, *156*, 519.
(145) Campione, M.; Tavazzi, S.; Moret, M.; Porzio, W. *J. Appl. Phys.* **2007**, *101*, 083512.
(146) Horowitz, G.; Bachet, B.; Yassar, A.; Lang, P.; Demanze, F.; Fave, J. L.; Garnier, F. *Chem. Mater.* **1995**, *7*, 1337.

(147) Siegrist, T.; Fleming, R. M.; Haddon, R. C.; Laudise, R. A.; Lovinger, A. J.; Katz, H. E.; Bridenbaugh, P.; Davis, D. D. *J. Mater. Res.* **1995**, *10*, 2170.
(148) Brillante, A.; Bilotti, I.; Biscarini, F.; Della Valle, R. G.; Venuti, E. *Chem. Phys.* **2006**, *328*, 125.
(149) Moulin, J.-F.; Dinelli, F.; Massi, M.; Albonetti, C.; Kshirsagar, R.; Biscarini, F. *Nucl. Instrum. Methods Phys. Res., Sect. B* **2006**, *246*, 122.
(150) Brillante, A.; Bilotti, I.; Albonetti, C.; Moulin, J.-F.; Stoliar, P; Biscarini, F.; de Leeuw, D. M. *Adv. Mater.* **2007**, *17*, 3119.
(151) Pan, H.; Liu, P.; Li, Y.; Wu, Y.; Ong, B. S.; Zhu, S.; Xu, G. *Adv. Mater.* **2007**, *19*, 3240.
(152) Cooper, W. F.; Kenny, N. C.; Edmonds, J. W.; Nagel, A.; Wudl, F.; Coppens, P. *J. Chem. Soc., Chem. Commun.* **1971**, *16*, 889.
(153) Ellern, A.; Bernstein, J.; Becker, J. Y.; Zamir, S.; Shahal, L.; Cohen, S. *Chem. Mater.* **1994**, *6*, 1378.
(154) Alves, H.; Molinari, A. S.; Xie, H. X.; Morpurgo, A. F. *Nat. Mater.* **2008**, *7*, 574.
(155) Brillante, A.; Bilotti, I.; Della Valle, R. G.; Venuti, E.; Milita, S.; Dionigi, C.; Borgatti, F.; Lazar, A. N.; Biscarini, F.; Mas-Torrent, M.; Oxtoby, N. S.; Crivillers, N.; Veciana, J.; Rovira, C. *CrystEngComm* **2008**, *10*, 1899.
(156) (a) Shibaeva, R. P.; Lobkovskaya, R. M.; Klyuev, V. N. *Cryst. Struct. Commun.* **1982**, *11*, 835. (b) Emge, T. J.; Wiygul, M.; Chappell, J. S.; Bloch, A. N.; Ferraris, J. P.; Cowan, D. O.; Kistenmacher, T. J. *Mol. Cryst. Liq. Cryst.* **1982**, *87*, 137.
(157) Mamada, M.; Yamashita, Y. *Acta Crystallogr., Sect. E* **2009**, *65*, O2083.
(158) Naraso; Nishida, J. I.; Ando, S.; Yamaguchi, J.; Itaka, K.; Koinuma, H.; Tada, H.; Tokito, S.; Yamashita, Y. *J. Am. Chem. Soc.* **2005**, *127*, 10142.
(159) Mas-Torrent, M.; Hadley, P.; Ribas, X.; Rovira, C. *Synth. Met.* **2004**, *146*, 265.
(160) Veres, J.; Ogier, S.; Lloyd, G. *Chem. Mater.* **2004**, *16*, 4543.
(161) Stassen, A. F.; de Boer, R. W. I.; Iosad, N. N.; Morpurgo, A. F. *Appl. Phys. Lett.* **2004**, *85*, 3899.
(162) Nicolas, G.; Martinelli, N. G.; Savini, M.; Muccioli, L.; Olivier, Y.; Castet, F.; Zannoni, C.; Beljonne, D.; Cornil, J. *Adv. Funct. Mater.* **2009**, *19*, 3254.
(163) (a) Gundlach, D. J.; Nichols, J. A.; Zhou, L.; Jackson, T. N. *Appl. Phys. Lett.* **2002**, *80*, 2925. (b) Kymissis, I.; Dimitrakopoulos, C. D.; Purushothaman, S. *IEEE Trans. Electron Devices* **2001**, *48*, 1060.
(164) Kelly, T.; Boardman, L. D.; Dunbar, T. D.; Muyres, D. V.; Pellerite, M. J.; Smith, T. P. *J. Phys. Chem. B* **2003**, *107*, 5877.
(165) Loi, M. A.; Da Como, E.; Dinelli, F.; Murgia, M.; Zamboni, R.; Biscarini, F.; Muccini, M. *Nat. Mater.* **2005**, *4*, 81.
(166) (a) Fritz, S. E.; Martin, S. M.; Frisbie, C. D.; Ward, M. D.; Toney, M. F. *J. Am. Chem. Soc.* **2004**, *126*, 4084. (b) Yang, H.; Shin, T. J.; Ling, M. M.; Cho, K.; Ryu, C. Y.; Bao, Z. *J. Am. Chem. Soc.* **2005**, *127*, 11542. (c) Kalihari, V.; Ellison, D. J.; Haugstad, G.; Frisbie, C. D. *Adv. Mater.* **2009**, *21*, 3092.
(167) Shehu, A.; Quiroga, S. D.; D'Angelo, P.; Albonetti, C.; Borgatti, F.; Murgia, M.; Scorzoni, A.; Stoliar, P.; Biscarini, F. *Phys. Rev. Lett.* **2010**, *10*, 246602.
(168) Dinelli, F.; Murgia, M.; Levy, P.; Cavallini, M.; Biscarini, F. *Phys. Rev. Lett.* **2004**, *92*, 116802.
(169) Li, L.; Gao, P.; Schuermann, K. C.; Ostendorp, S.; Wang, W.; Du, C.; Lei, Y.; Fuchs, H.; De Cola, L.; Müllen, K.; Chi, L. *J. Am. Chem. Soc.* **2010**, *132*, 8807.
(170) (a) Malenfant, P. R. L.; Dimitrakopoulos, C. D.; Gelorme, J. D.; Kosbar, L. L.; Graham, T. O.; Curioni, A.; Andreoni, W. *Appl. Phys. Lett.* **2002**, *80*, 2517. (b) Ostrick, J. R.; Dodabalapur, A.; Torsi, L.; Lovinger, A. J.; Kwock, E. W.; Tiller, T. M.; Galvin, M.; Berggren, M.; Katz, H. H. *J. Appl. Phys.* **1997**, *81*, 6804.
(171) Tulevski, G. S.; Miao, Q.; Fukuto, M.; Abram, R.; Ocko, B.; Pindak, R.; Steigerwald, M. L.; Kagan, C. R.; Nuckolls, C. *J. Am. Chem. Soc.* **2004**, *126*, 15048.
(172) Guo, X.; Myers, M.; Xiao, S.; Lefenfeld, M.; Steiner, R.; Tulevski, G. S.; Tang, J.; Baumert, J.; Leibfarth, F.; Yardley, J. T.; Steigerwald, M. L.; Kim, P.; Nuckolls, C. *Proc. Natl. Acad. Sci. U.S.A.* **2006**, *103*, 11452.
(173) Mottaghi, M.; Lang, P.; Rodriguez, F.; Rumyantseva, A.; Yassar, A.; Horowitz, G.; Lenfant, S.; Tondelier, D.; Vuillaume, D. *Adv. Funct. Mater.* **2007**, *17*, 597.
(174) Smits, E. C. P.; Mathijssen, S. G. J.; van Hal, P. A.; Setayesh, S.; Geuns, T. C. T.; Mutsaers, K. A. H. A.; Cantatore, E.; Wondergem, H. J.; Werzer, O.; Resel, R.; Kemerink, M.; Kirchmeyer, S.; Muzafarov, A. M.; Ponomarenko, S. A.; de Boer, B.; Blom, P. W. M.; de Leeuw, D. M. *Nature* **2008**, *17*, 597.
(175) Spijkman, M.; Mathijssen, S. G. J.; Smits, E. C. P.; Kemerink, M.; Blom, P. W. M.; de Leeuw, D. M. *Appl. Phys. Lett.* **2010**, *96*, 143304.
(176) Campione, M. *J. Phys. Chem. C* **2008**, *112*, 16178.
(177) (a) Seo, J.-H.; Park, D.-S.; Cho, S.-W.; Kim, C.-Y.; Jang, W.-C.; Whang, C.-N.; Yoo, K.-H.; Chang, G.-S.; Pedersen, T.; Moewes, A.; Chae, K.-H.; Cho, S.-J. *Appl. Phys. Lett.* **2006**, *89*, 163505. (b) Hu, W.-S.; Weng, S.-Z.; Tao, Y.-T.; Liu, H.-J.; Lee, H.-Y. *Org. Electron.* **2008**, *9*, 385.
(178) Li, Z.; Du, J.; Tang, Q.; Wang, F.; Xu, J.-B.; Yu, J. C.; Miao, Q. *Adv. Mater.* **2010**, *22*, 3242.
(179) Dholakia, G. R.; Meyyappan, M.; Facchetti, A.; Marks, T. J. *Nano Lett.* **2006**, *6*, 2447.
(180) Asadi, K.; Wu, Y.; Gholamrezaie, F.; Rudolf, P.; Blom, P. W. M. *Adv. Funct. Mater.* **2009**, *21*, 4109.
(181) Stoliar, P.; Kshirsagar, R.; Massi, M.; Annibale, P.; Albonetti, C.; de Leeuw, D. M.; Biscarini, F. *J. Am. Chem. Soc.* **2007**, *129*, 6477.